

Article

# Selected Aspects of Designing Modular PEMFC Stacks as Power Sources for Unmanned Aerial Vehicles

Magdalena Dudek <sup>1,\*</sup> , Bartłomiej Lis <sup>1</sup>, Andrzej Raźniak <sup>1</sup> , Mariusz Krauz <sup>2</sup> and Michał Kawalec <sup>2</sup>

<sup>1</sup> Faculty of Energy and Fuels, AGH University of Science and Technology, Al. A. Mickiewicza 30, PL 30059 Krakow, Poland; blis@agh.edu.pl (B.L.); razniak@agh.edu.pl (A.R.)

<sup>2</sup> Institute of Power Engineering Ceramic Department CEREL, Techniczna 1 St, PL 36040 Boguchwala, Poland; krauz@cerel.pl (M.K.); mich.kawalec@gmail.com (M.K.)

\* Correspondence: potoczek@agh.edu.pl

**Abstract:** Two types of air-cooled modular polymer membrane fuel cells (PEMFC) stacks with full equipment were constructed and investigated as components of hybrid power sources. The first, a 2-kW PEMFC stack, was assembled from two 1-kW PEMFC modules electrically connected in parallel and compared with a commercial PEMFC stack built from one 2-kW PEMFC module. The second, a 500-W PEMFC stack, was assembled with three modules connected in parallel. It was found that the two-module PEMFC stack was capable of operation with nominal power of 2 kW. Analysis of the distribution of the air cooling system in both modules was also conducted. The two-module PEMFC stack reduced hydrogen consumption compared to the reference 2-kW PEMFC stack consisting of only one module. The elaborated two-module PEMFC stack was successfully tested in a propulsion system designed to supply an electrical engine with a propeller. The electrical performance of the three-module PEMFC stack was tested separately as well as in a hybrid system in connection with a 5 s Li-Pol battery. It was found that the elaborated PEMFC stack was capable of operation with nominal power of 500 W and variable rapid dynamic electrical loads. It was also successfully tested as a power source to supply servomechanisms and other auxiliary devices.

**Keywords:** PEMFC fuel cell stack; hydrogen; unmanned aerial vehicles; modular power source



**Citation:** Dudek, M.; Lis, B.; Raźniak, A.; Krauz, M.; Kawalec, M. Selected Aspects of Designing Modular PEMFC Stacks as Power Sources for Unmanned Aerial Vehicles. *Appl. Sci.* **2021**, *11*, 675. <https://doi.org/10.3390/app11020675>

Received: 18 December 2020

Accepted: 8 January 2021

Published: 12 January 2021

**Publisher's Note:** MDPI stays neutral with regard to jurisdictional claims in published maps and institutional affiliations.



**Copyright:** © 2021 by the authors. Licensee MDPI, Basel, Switzerland. This article is an open access article distributed under the terms and conditions of the Creative Commons Attribution (CC BY) license (<https://creativecommons.org/licenses/by/4.0/>).

## 1. Introduction

In recent years, unmanned aerial vehicles (UAVs) have become more and more widely used for civil, rescue, and military applications. Drones are flying machines, included in the category of UAVs, which fly autonomously or are remotely piloted from the ground by an operator. Advances in design, the construction of flying robots, and progress in navigation, remote control capabilities, and power storage systems have enabled the design and development of different types of fully equipped UAVs, which can find new potential applications in challenging environments [1,2]. In such missions, human involvement may be difficult, impossible, or dangerous, usually leading to risks to life or health. Reductions in operating costs and minimization of infrastructure requirements may also be among the benefits of the use of drone technology [3,4]. The category of drone applications depends on the drone's mission (military, civil), types of flight zones (outdoor, indoor), and types of environments (underwater, water, ground, air, space). UAVs used for military applications can accomplish special tasks such as firing missiles, dropping bombs, making camouflaged flights, disrupting communications, transporting medical supplies to battlefields, operating as invisible spies, maintaining surveillance, conducting planetary exploration, and providing search and rescue services. Depending on the flight mission of UAVs, their construction and size, and the type of equipment installed on board, power sources are required for both primary propulsion and auxiliary systems [5–10]. Electrochemical battery-powered electrical motors are the most popular choices for small and mid-sized drones. Another option for electrical engines is represented by application of hydrogen-oxygen fuel cells,

electrochemical devices which directly convert the chemical energy of fuel (mainly hydrogen) into electricity. These devices can be operated for as long as reagents (especially fuel) can be supplied. The operating time of power sources involving fuel cells depends on their level of electric power consumption and the amount of hydrogen stored [11–13]. For UAV applications based on quiet operation, improved safety, and precise power management and control, which involve the coverage of longer distances and superior performance in harsh conditions, and also considering the reduction of pollutants and greenhouse gas emissions, the application of hydrogen in fuel cells for electrical propulsion appears to be preferred [14–18]. In drone applications, fuel cells are limited in their ability to provide the required power for maneuvers: take off, climbing or flight under variable atmospheric conditions. When the power load profile varies greatly, some unpleasant phenomena may occur in hydrogen-oxygen fuel cells: (i) local dehydration of Nafion-based membrane electrode assembly (MEA), (ii) membrane flooding, or (iii) reactant starvation. These lead to a reduction in the durability and lifetime of the fuel cells.

The polymer membrane fuel cells (PEMFC) should be hybridized with high-discharge lithium batteries. The battery can also be charged to keep SOC above the prescribed limit. Hybrid electric control system in such power sources can be active or passive. Active systems use energy control and management strategies based on DC/DC converters, while passive ones adjust the voltages of the different power sources at the main DC bus either by direct connection or by using power diodes [19–21]. The commercial AeroStack hybrid power source involving a 200 W PEMFC stack was the most frequently studied hybrid power source unit. It was discovered that the battery has considerable importance on the hybrid power system during dynamic variable electrical loads. The battery protected the PEMFC fuel cells during operation under considerable increase of electrical load, which could lead to faster damage or operation in the low efficiency region [22–24]. Zhang, et al. showed that when hybrid power sources are used in the propulsion system, the hydrogen consumption of the fuel cell can be reduced using an energy management system [25]. The number of completed and fully equipped drones powered by commercial hybrid electric propulsion systems (each of which consists of a PEMFC fuel cell and battery) has also gradually increased. A Hycopter powered by PEMFCs (HES Energy Systems, Horizon, Singapore) flew for over 4 h. Energyor, Technologies Inc., Montreal, Quebec, Canada) presented a multirotor vehicle in which the use of PEMFCs enabled a flight of over 2 h. Other successful tests include those conducted by MMC, a Chinese manufacturer of drones, and Intelligent Energy, incorporating fuel cells into UAV designs and extending flight times from 2 to more than 4 h [26–30]. The use of hydrogen-powered fuel cells in hybrid power systems, in addition to extending flight time compared to only battery-powered systems, has an additional advantage that increases their operability: hydrogen tanks can be refueled within a few minutes so that the UAV can perform its next mission; unlike in the case of electrochemical batteries, which must be recharged for several hours to be reused, or must be replaced with new extra battery cell packages [31]. With regard to the commercial solutions listed in papers [26–30], efforts undertaken in many aerospace or fuel cell research laboratories are also focused on conducting a series of modelling and simulations concerning optimization of PEMFC stack performance in hybrid power sources under UAV flight. Most of these are also confirmed by experimental investigations in stationary conditions by testing under variable electrical loads [32–34]. The increase in durability of PEMFC stacks under variable electrical loads in different conditions is one of the main strategical goals for developing the technology of hybrid propulsion systems for application in UAVs. The increase of durability of the PEMFC stack under variable electrical loads in different conditions is one of main strategical goals for the developing technology of hybrid propulsion systems for UAV applications.

The main components of the energy system in an electrical hybrid propulsion system comprise an electrochemical battery, hydrogen-oxygen fuel cells, and DC-DC converters. In some cases the range of electrical voltage during PEMFC stack operation is not compatible with the electrical architecture of the current electrical engine system. Within this

framework, multistack fuel cell (MCFC) systems may be possible solutions. Indeed, when associated with specific electrical flowing reagents and coolant architecture, MCFC systems may offer superior performance in terms of power output and system durability. In the case of inferior electrical operation due to the presence of degraded cells in the module, the system may still be reliable thanks to the redundancy of other PEMFC modules. Modular fuel cell stacks have been used in air-independent propulsion for submarine power supplies and for space exploration vehicles [35–38]. The results of electrical properties and durability of a modular PEMFC stack designed as part of a hybrid source for use in a propulsion system designed to supply an electrical engine in a motor glider or Antares DLR-H<sub>2</sub> research aircraft [39,40].

The goal of the paper is to present selected results concentrating on the construction and electrical performance of modular polymer membrane fuel cell stacks as components of hybrid power sources capable of application in drones. One power source is a device composed of two identical subunits, each consisting of a 1-kW fuel cell stack, intended to supply power to the main electric engine. The other power source is a 500-W PEMFC stack, consisting of three modules, intended to serve as a component of a hybrid power source designed to supply auxiliary on-board equipment. A detailed analysis of relevant electrical performance, cooling systems, the use of hydrogen fuel, and durability is presented, along with a comparison with a classical solution based on a single-module PEMFC stack.

## 2. Experimental Parts

### 2.1. Description of Designed and Assembled Modular PEMFC Stacks

#### 2.1.1. First Power Source: A 2000-W PEMFC Stack Constructed from Two 1-kW Modules Electrically Connected in Parallel

The first power source (I) was a 2-kW PEMFC stack consisting of two fuel cell modules connected in parallel, each containing 44 single MEAs connected in series.

Bipolar graphite plates were applied. All modular PEMFC stacks were cooled by air. In each stack, the end plates compressing individual MEAs were made of carbon-epoxy laminate. The MEAs consisted of Nafion 112 membranes, catalyst layers with a total Pt loading of 0.4 mg cm<sup>2</sup> at both anode and cathode sides and SGL carbon with a microporous layer as gas diffusion layers (GDL) were commercially supplied by Fuel Cell Store. The active area of each MEA is ~58.9 cm<sup>2</sup>. The dimensions of the graphite bipolar plates used for assembling the PEMFC stack are 196 mm × 30 mm × 2.2 mm.

These plates were compressed using threaded rods which ensured the required degree of tightness in each module. As shown in Figure 1a,b, the 2-kW PEMFC stack consisted of two fuel cell modules, (1) and (2), connected in parallel. High-current Schottky diodes were used to protect the individual stacks from reverse polarity caused by inconsistent operating conditions. The system was equipped with two independent microcontroller unit systems for management of the parallel-connected (1) and (2) modules of the PEMFC stack. The operation of the air cooling fans was controlled by means of a feedback loop based on the measurement of the temperature inside modules (1) and (2). The operating temperature of each module was set at 55 °C. Air fans (Sunon model PF9225), dimensions: 92 mm × 92 mm × 25 mm, each with electrical power of ~5 W and maximum air flow of 120 m<sup>3</sup>/h were selected for the construction of the cooling system. Four fans were installed in each module. Hydrogen was supplied first to a common pressure regulator, then independently to modules (1) and (2).

#### 2.1.2. Second Power Source: A 500-W PEMFC Stack with Three Modules Connected in Parallel

As shown in Figure 2a–c, the other PEMFC stack consisted of three fuel cell modules (1–3), each module consisting of 44 single MEAs connected in series. The MEAs consisted of Nafion 112 membranes, catalyst layers with a total Pt loading of 0.4 mg cm<sup>2</sup> on anode and cathode sides and SGL carbon with microporous layer as gas diffusion layers (GDL) were commercially supplied by Fuel Cell Store. The dimensions of the graphite bipolar plates used for the assembling PEMFC stack were 100 mm × 30 mm × 1.2 mm. The active

area of each MEA was  $\sim 25 \text{ cm}^2$ . Copper-coated glass/epoxy laminate separation plates were placed between the modules. The copper layer was protected from corrosion by a layer of gold. Hydrogen under 0.5 bar of pressure was supplied successively to all MEAs in each module through an internal insulated duct. To supply the cooling air and oxygen flow required for the cathode reaction, five axial fans were used. The rotational speed of the fans was monitored by the PEMFC stack central microcontroller unit (MCU), which calculated the control signal based on the temperature measurements of the individual modules from the stack and management of the performance of the complete unit. The elaborated microcontroller unit managed the purge valves and the operation of the short-circuit units (SCUs) and monitored the levels of voltage and current of individual modules 1–3. The modular 500-W fuel cell stack was connected in parallel to a lithium polymer battery (5–9 s) through a charge–discharge process control board.

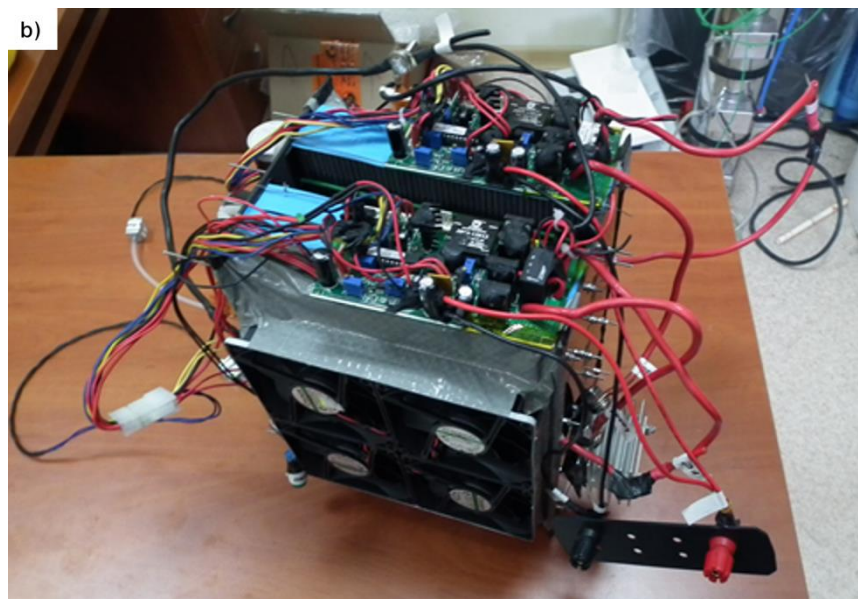
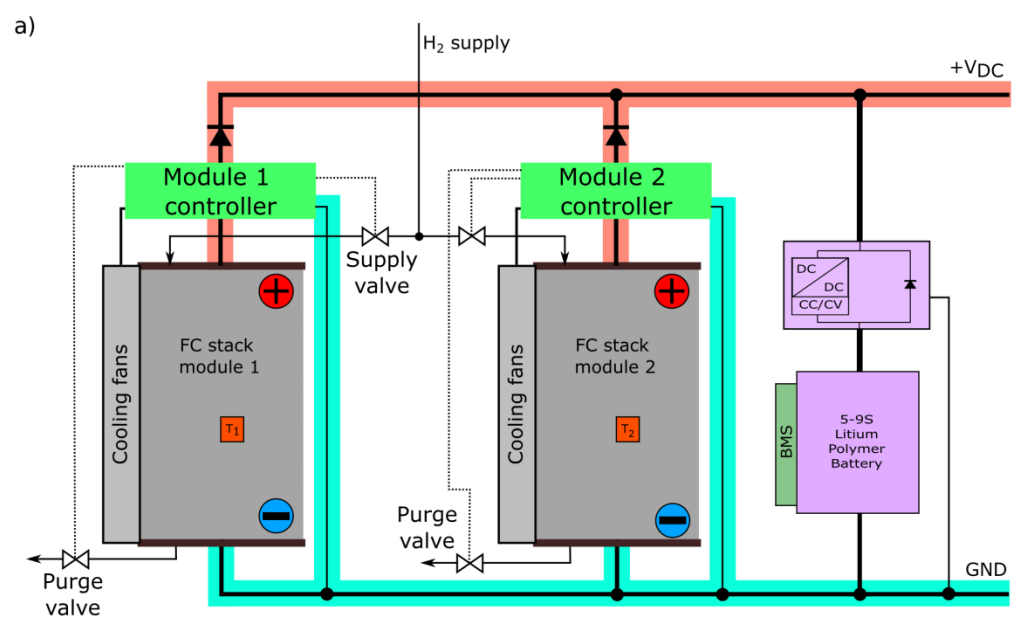


**Figure 1.** (a) The 2-kW polymer membrane fuel cell (PEMFC) stack consisting of two fuel cell modules, (1) and (2) connected in parallel with a potential connection to an electrochemical battery. (b) The photo of 2-kW PEMFC stack consisting of two fuel cell modules.

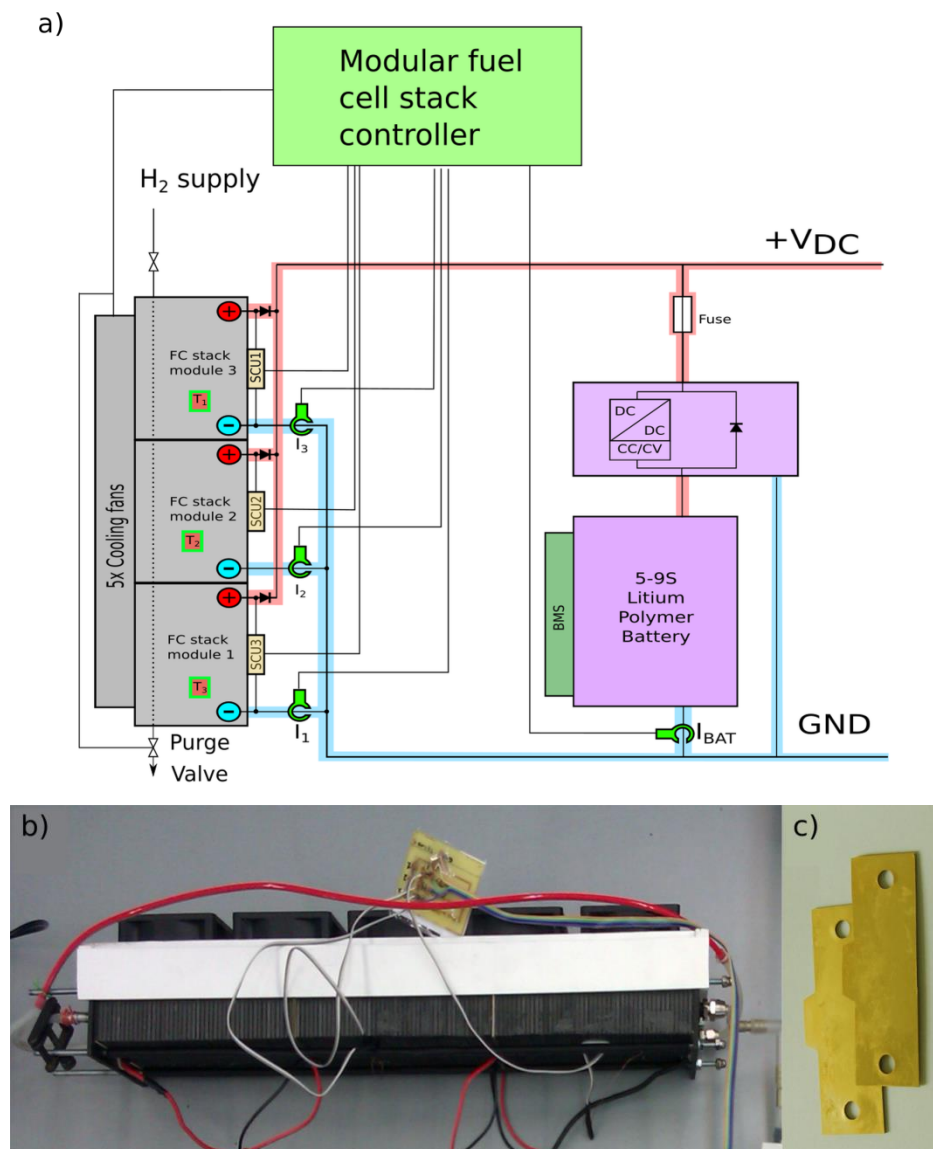


**Figure 2.** (a) A 0.5-kW PEMFC stack consisting of three fuel cell modules (1–3) connected in parallel with a potential connection to an electrochemical battery. The photos of (b) the 3-modular PEMFC stack and (c) copper-coated glass/epoxy laminate separation plates.

## 2.2. Method of Measurement and Measuring Equipment Used

The U-I and P-I curves for the 2000-W power source (I) were measured using electrochemical stations (CLB-2000, BioLogic, Claix, France, 2 kW) equipped with electronic load. In the case of power source (II) with 500-W modular PEMFC stacks, a programmable electronic load (Dynaload XBL 50-150-800, TDI Power, Hackettstown, NJ, USA) was used along with an electrochemical interface (FC350 Fuel Cell Interface, Gamry, Warminster, PA, USA). Variations in current (I) and voltage (U) during operation of the humidification implemented by the SCU system were measured using the oscilloscopic method (DS1062CA digital oscilloscope, Rigol, Suzhou, China). During the operation of both investigated PEMFC stacks, total consumption of hydrogen was measured using a digital electronic mass flow meter (EL-Flow, Bronkhorst High-Tech, Ruurlo, The Netherlands). The hydrogen pressure supplied to the stacks was monitored by an electronic pressure regulator (EL-PRESS, Bronkhorst High-Tech, Ruurlo, The Netherlands). The resulting values were saved on the computer for further analysis. Measurements of the electrical parameters of 1000-W PEMFC modules (1) and (2) used for the construction of power source (I) were

conducted using electrochemical impedance spectroscopy (EIS). The main component of the station was an electronic load (Dynaload XBL 50-150-800), which enabled strictly controlled current loading and determination of impedance spectra via EIS using fuel cell stack test cards (Gamry, Warminster, PA, USA). The electronic load was controlled from a PC, which simultaneously collected measurement data. Measurements were carried out at four fixed DC values (1, 10, 16, and 25 A) over which a small variable sinusoidal load was applied. The impedance of the 1-kW PEMFC module was determined for a frequency within the range 10 kHz–0.1 Hz. The recorded voltage was used to determine the impedance spectra. The commercial software ZPlot (Scribner, New York, NY, USA) was used to fit an equation describing the assumed equivalent electrical circuit (EEC) to the measured data. The hydrogen necessary to operate the fuel cell was supplied from the gas installation as well as from two composite bottles ( $2 \times 6.8 \text{ dm}^3$ , supplier Horizon, Fuel Cell Technologies, Singapore) and pressure was reduced to 0.5 bar. The amount of compressed hydrogen storage in the two composite cylinders of the 2-kW PEMFC stack or in the  $1 \text{ dm}^3$  ultra-light cylinder for the 500-W PEMFC stack was monitored by AST2000H2 hydrogen pressure sensors (American Sensor Technologies, Inc., Budd Lake, NJ, USA). The temperature of the PEMFC stack during operation was monitored by Pt1000 resistance temperature sensors located inside modules (1) and (2). Signals from temperature measurement, on the basis of which the operation of the cooling fans was monitored, were sent to the PEMFC controller. During the electric measurements, the energy consumption of the auxiliary devices was analyzed and the measurements monitored. Using a Power Log 6S logger, the parameters (voltage, current, and power) of the fan system cooling the stack were recorded. The temperature distribution was also measured by a thermal imaging camera (Thermo Tracer NEC H2640) (Figure 3). Thermal images were recorded, following the determination of the stack temperature under a load of 800 W, on an uncovered side surface of the two-module PEMFC stack.

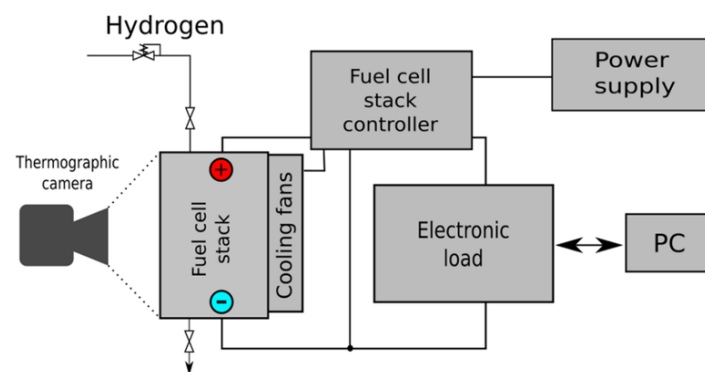


**Figure 3.** The 1-kW PEMFC module (1) or (2) during EIS investigations performed online with temperature distribution measured with a thermographic camera.

Single-module 2-kW PEMFC stacks, such as a BCH Energy 2000 (Jiangsu Ice-City Hydrogen Energy Technology Co., Ltd., Danyang, China) and a Horizon 2000 PEMFC stack from H-series, were chosen as reference devices in order to compare their performance with the newly-built two-module PEMFC stacks (2M). The BCH Energy 2000 (BCH) was also constructed from Nafion-based membranes; metallic bipolar plates were used. This unit was designed for direct application in drones [41]. In the case of the H2000 PEMFC stack, graphite-bipolar plates (HG) were used, but the electrical U-I and P-I characteristics are also similar to those of an Aerostak series fuel cell stack recommended for drone applications [42]. In subsequent investigations, the elaborated two-module 2-kW PEMFC stack was investigated using laboratory electrical propulsion systems such as the one shown in Figure 4.

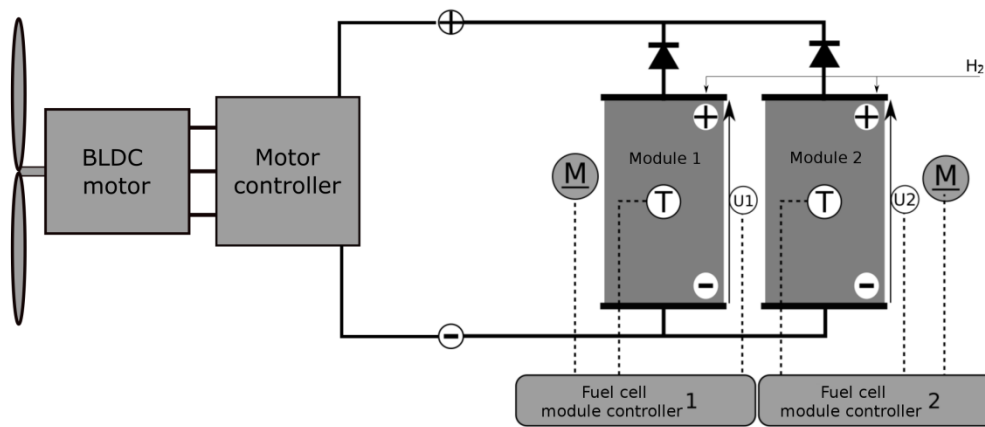


Figure 4. Design of an electrical setup to test the constructed 2000-W PEMFC stack connected with a propulsion unit.

A brushless direct-current motor (BLDC) was used for these stationary laboratory tests. The electric motor was connected first to a propeller (30 × 12) and then to the constructed 2-kW PEMFC stack as a power source. During the measurement, the rotational speed of the electrical motor was gradually increased while the electric power drawn from power source (I) (two PEMFC fuel cell modules (1) and (2) connected in parallel) was being recorded.

In the next stage, the 500-W PEMFC stack was tested as an auxiliary power source to supply servomechanisms, such as the one shown in Figure 5. To investigate this device in conditions approximating those of an actual application, an experimental servo setup was constructed, consisting of an L 13 BLANIK (BH135) model airplane with installed servos. A BH135 aircraft was equipped with an Aeronaut CAM carbon 16 × 8 mm propeller, an AXi 4130/20 electrical engine, a remote-control system, five servos, and two mini-servos. The servos were installed, enabling control of the hatches, rudder, engine, aileron, and elevator. The performance of the servo operations supplied by the 500-W PEMFC stack was tested using an E-Sky 000537 Servo Tester. This device imitated the output impulses of the remote controller, enabling the servos to be tested without installing a remote-control system each time.

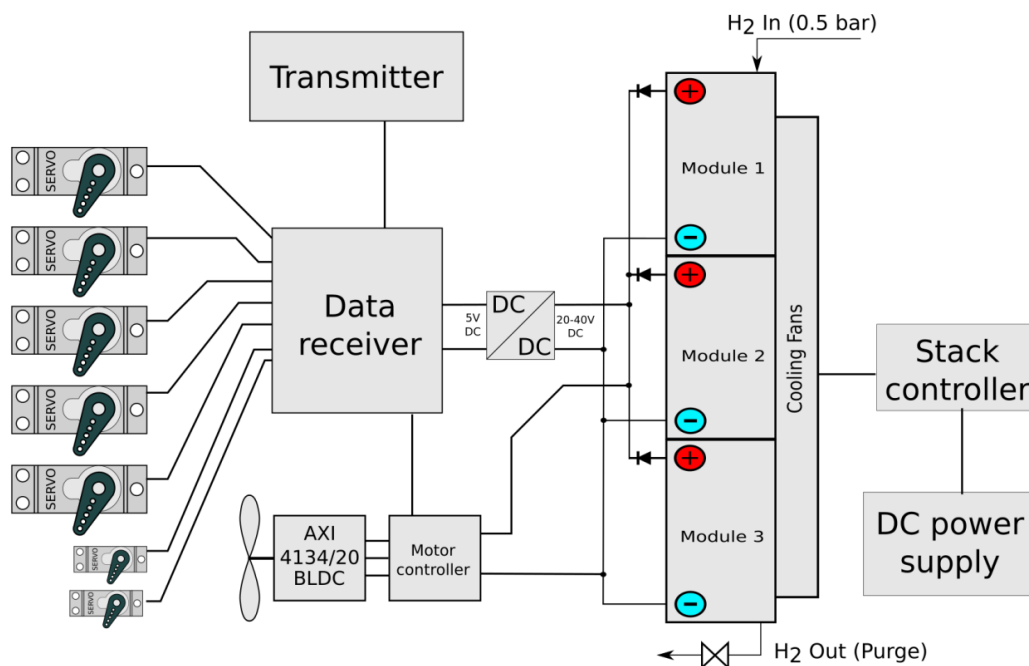
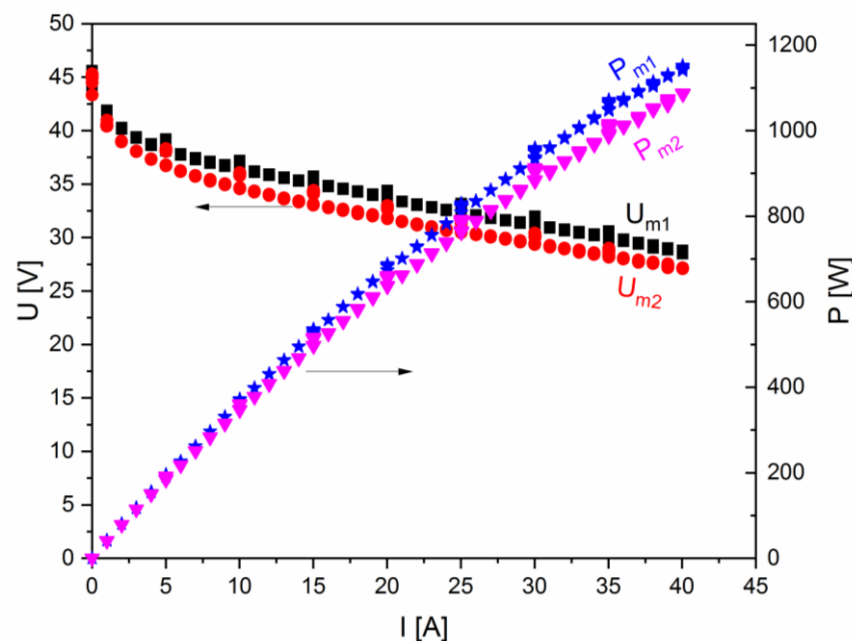


Figure 5. Diagram of a 500-W modular fuel cell stack integrated with UAV on-board flight control devices.

### 3. Results

#### 3.1. Electrical Tests of the Designed Two-Module 2-kW PEMFC Stack

In accordance with the requirements of the electrical propulsion system, it was necessary to maintain operation of the PEMFC stack within the voltage range 28–38 V. The dimensions and combined weight of the two modular stacks were limited by the construction and dimension of the UAV's fuselage. Our design of the 2-kW PEMFC stack met the requirements of the electrical propulsion system; it proved efficacious to construct it from smaller modules. The elaborated stack was assembled from two 1-kW modules, each consisting of 44 single MEAs. The two 1-kW modules, electrically connected in parallel, possessed two independent microcontroller system units (MCU), one for each module. Prior to the connection of modules (1) and (2) as one 2000-W power source (I), the U-I and P-I curves were recorded for each module independently. Figure 6 presents the voltage (U)-current (I) and power (P)-current (I) curves recorded for modules (1) and (2).



**Figure 6.** Voltage (U)-current (I) and power (P)-current (I) curves recorded for independent 1-kW modules 1 ( $U_{m1}$ ,  $P_{m1}$ ) and 2 ( $U_{m2}$ ,  $P_{m2}$ ) prior to electrical connection in parallel.

The obtained voltage (U)-current (I) and power (P)-current (I) curves indicated that the two constructed 1-kW modules exhibited similar electrical parameters. Nominal power output  $P_{nom}$  was higher than the assumed level of 1000 W, equaling  $P_{m1} = 1152$  W and  $P_{m2} = 1087$  W for modules (1) and (2), respectively. This data indicated that both modules could be applied via parallel electrical connections to obtain total nominal power of 2 kW.

Electrochemical impedance spectroscopy (EIS) was also applied to the study of variations in the electrical resistance of 1-kW module (1) or (2) prior to its electrical connection in parallel to the designed 2-kW PEMFC stack. The measurements were performed under different electrical loads. Figure 7a,b presents the  $Z'-Z''$  diagrams for modules (1) and (2). The EIS spectra recorded for PEMFC modules can be numerically fitted by the equivalent circuit shown in Figure 7c. The high frequency intercept part (intersection with the real axis in impedance spectrum) reflects the ohmic resistance ( $R_{\Omega}$ ) of PEMFC module (1) or (2); the arc at medium frequency reflects the combination of charge transfer ( $R_{ct}$ ) due to the oxygen reduction reaction and double layer capacitance within the catalyst layer, which is considered to be a constant phase element ( $CPE_1$ ), the arc at low frequency reflects the mass transport resistance of oxygen in the catalyst layer ( $R_m$ ) and the associated constant phase element ( $CPE_2$ ). The anodic polarization is very small and can be ignored. Thus,

the obtained impedance spectrum mainly reflects the cathode polarization. The described equivalent electrical circuit is often applied to EIS analysis of PEMFC stacks [43–45].

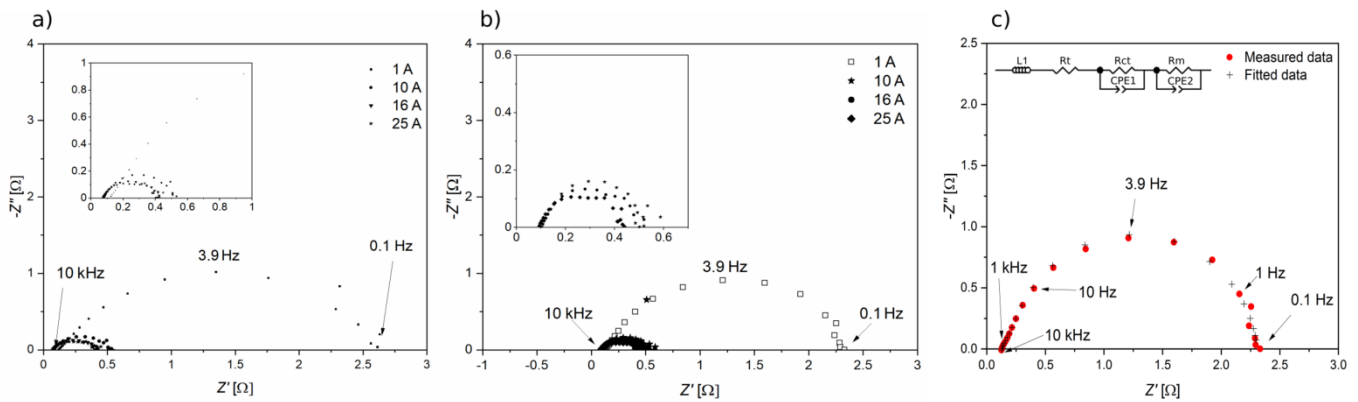


**Figure 7.** (a,b) Impedance spectra recorded for 1-kW PEMFC module (1) or (2) under applied electrical loads:  $I = 1, 10, 16,$  and  $25$  A, and (c) example of equivalent electrical circuit used to analyze the impedance spectra,  $L$  is the pseudo-inductance,  $R_{\Omega}$ —ohmic resistance,  $R_{ct}$ —charge transfer resistance,  $R_m$ —mass transport resistance,  $CPE_1$  and  $CPE_2$ —constant phase elements connected in parallel with  $R_{ct}$  and  $R_m$ .

An ohmic resistance  $R_{\Omega}$ , charge transfer resistance  $R_{ct}$ ,  $R_m$ —mass transport resistance and total electrical resistance  $R_t$  calculated as a sum of  $(R_{ct} + R_m + R_{\Omega})$  (Figure 8a,b) decreased along with an increase in the electrical load. One possible explanation for this phenomenon is the gradual humidification of the Nafion-polymer electrolyte. An increase in humidity level due to the operation of the PEMFC module with a higher electrical load caused the presence of water in the fuel cell area. This reduced the total electrical resistance of the PEMFC stack and improved the kinetics of the electrode processes ( $R_{ct}$ ) and mass transport ( $R_m$ ) in the PEMFC modules due to an increase in temperature. These statements are in close agreement with data obtained from U-I curves.

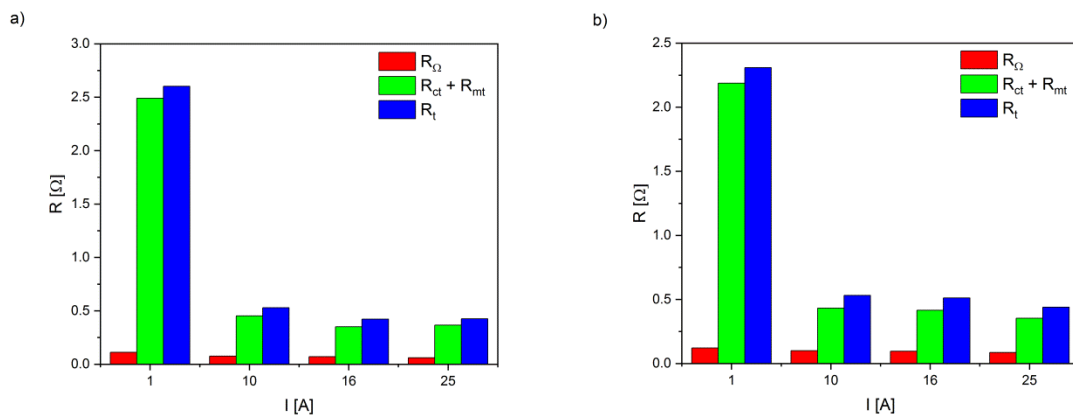


**Figure 8.** (a,b) The variation of resistances:  $R_{\Omega}$ ,  $(R_{ct} + R_m)$  or  $R_t$  vs. applied electrical load recorded for PEMFC modules (1) and (2).

The operation of the PEMFC module under a higher electrical load caused an increase in temperature from  $\sim 24$  to  $\sim 50$  °C. The temperature distribution measured via thermographic camera (in accordance with the experimental setup presented in Figure 3) in a 1-kW PEMFC module operating under an electrical load of  $I = 25$  A is presented in Figure 9.

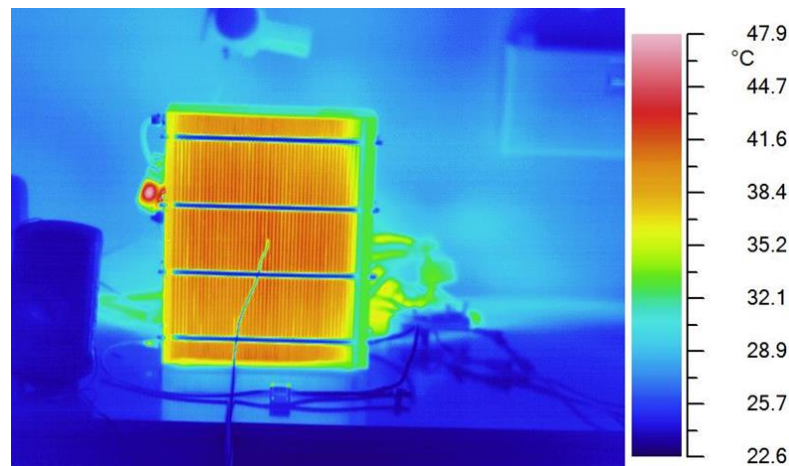


**Figure 9.** The temperature distribution in 1-kW PEMFC module (1) operating under an electrical load of  $I = 25$  A, measured via thermographic camera.

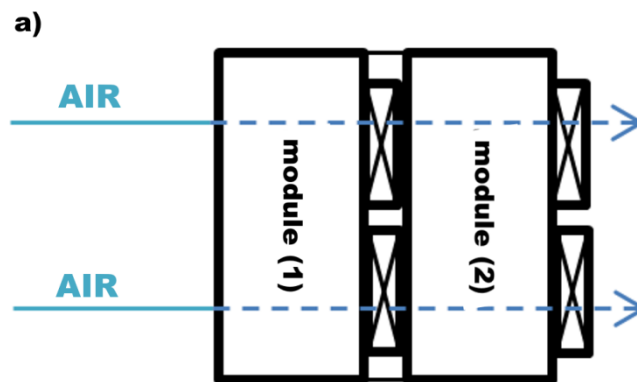
Cooling air was supplied to modules (1) and (2) by air axial fans. Four fans were installed in each 1-kW PEMFC module. The maximum air flow capacity for modules (1) and (2) was  $8 * 120 \text{ m}^3/\text{h} = 960 \text{ m}^3/\text{h}$ , which, given the difference in the temperature of the flowing cooling air of  $10 \text{ }^\circ\text{C}$ , enabled the discharge of 2650 W of heat. This value is sufficient to cool a 2-kW fuel cell stack.

$$Q = \dot{V} \cdot \rho \cdot C_{pp} \cdot \Delta T \tag{1}$$

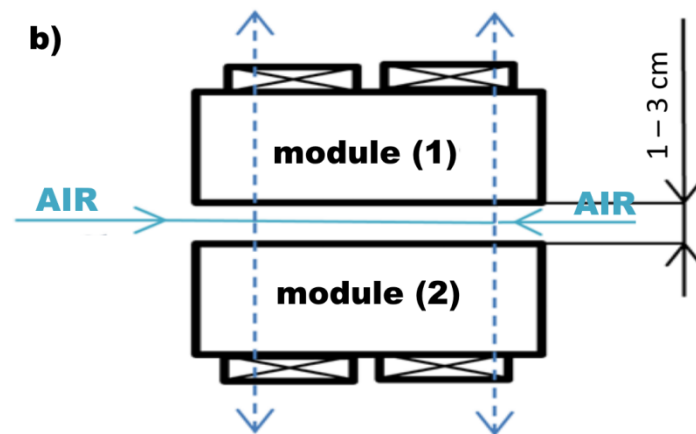
$$Q = 8 \cdot 120 \frac{\text{m}^3}{\text{h}} \cdot 1 \frac{\text{h}}{3600\text{s}} \cdot 1.3 \frac{\text{kg}}{\text{m}^3} \cdot 1020 \frac{\text{J}}{\text{kg} \cdot \text{K}} \cdot 10\text{K} = 2650\text{W} \tag{2}$$

where:  $Q$  is the heat picked up by the cooling air;  $\dot{V}$  is the stream of air;  $\rho$  is the air density.  $C_{pp}$  is the specific heat of the air;  $\Delta T$  is the temperature difference between the inlet and outlet of the cooling air.

The concept of parallel vs. series air flow through electrically connected modules (1) and (2) is presented in Figure 10a,b.



**Figure 10.** Cont.



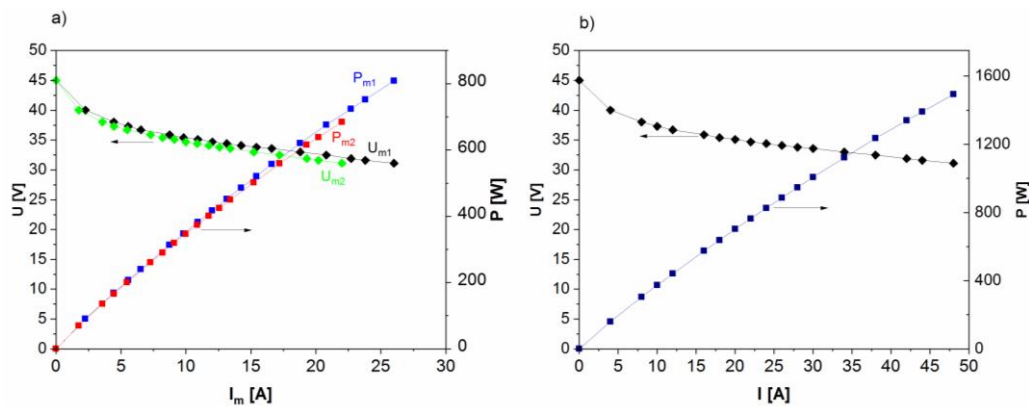
**Figure 10.** Cooling air flow through modules (1) and (2) arranged in (a) series or (b) parallel.

Figure 10a presents a situation in which cooling air flows through modules (1) and (2) arranged in series. Air at ambient temperature was drawn from outside into cool module (1), where it received heat and moisture ( $H_2O$ ) released by the cathode. This preheated air, which flowed through module (2) only, was discharged outside after it had cooled down and taken the moisture from module (2). In this cooling configuration, modules (1) and (2) were characterized by different cooling conditions, as module (1) was directly cooled with ambient air from the surroundings, while module (2) was cooled with air that had already been preheated in module (1) and thus was at a higher temperature. In this unfavourable situation, the control system of the cooling fans must force the greater air flow necessary to cool module (2). Increased cooling air flow can lead to a temperature gradient in the module, which may be directly caused by increased moisture loss through selected MEA cells or by the presence of MEA cells at much higher temperatures than the others in the module. This phenomenon causes a higher level of energy consumption for cooling module (2) than for module (1). In addition, it can lead to more rapid degradation of individual cells in module (2).

Figure 10b, on the other hand, presents cooling air flow through modules (1) and (2) arranged in parallel. The situation was different in this arrangement of modules (1) and (2), where air was drawn into the fans from outside, from the space between modules (1) and (2), which were arranged in parallel at a distance of 3 cm. This air, after taking on the excess heat and moisture released during operation, was discharged outside to the environment. In this configuration, modules (1) and (2) were characterized by the same cooling conditions and were cooled more evenly than in Figure 10a; accordingly, this cooling configuration was the preferable solution.

Figure 11 presents the U-I and P-I curves recorded for the designed 2-kW PEMFC stack, assembled from two modules, where cooling air flowed through modules (1) and (2) according to situation from Figure 10a.

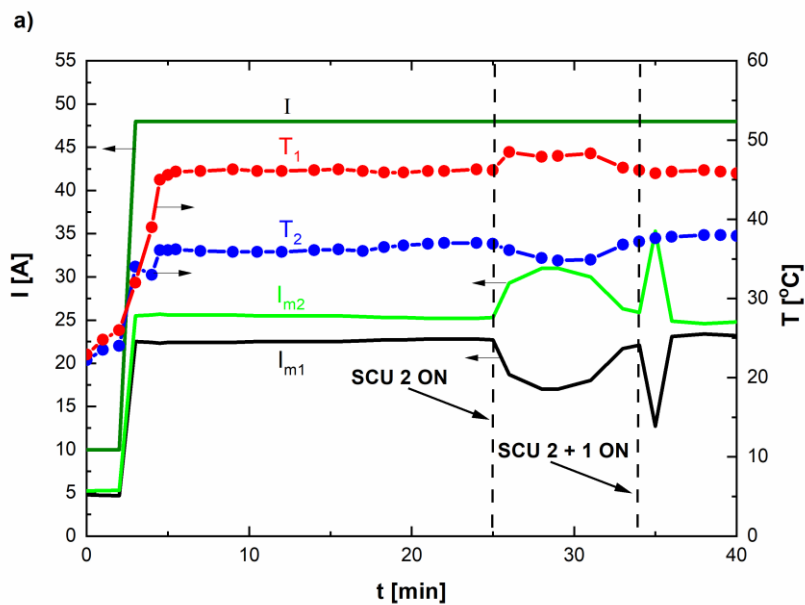
Direct comparison of U-I and P-I curves recorded for modules operated as independent components of the 2-kW PEMFC stack (Figure 6) with those recorded for the same modules where cooling air flows through the two modules (1) and (2) arranged in series indicated that in the situation presented in Figure 10a, the level of electrical performance (Figure 11a,b) is slightly lower. A lower value of maximum electrical power  $P$  was reached for both modules compared to the original experimental data. In this situation the total power recorded for the two-module PEMFC stack was less than 2000 W.



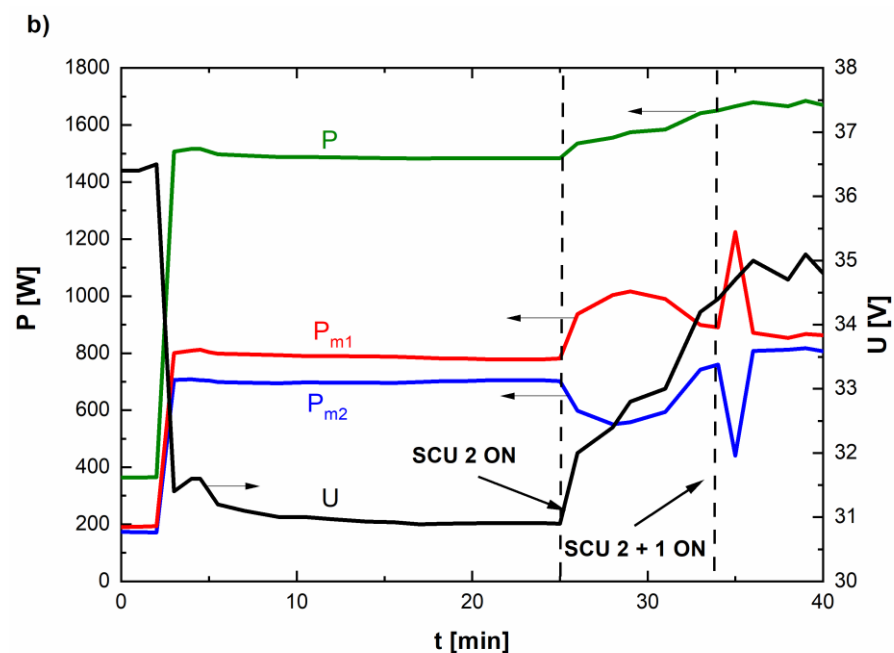
**Figure 11.** (a) Voltage ( $U$ )-current ( $I_m$ ) and power ( $P$ )-current ( $I_m$ ) curves recorded for individual fuel cell modules (1) and (2) which are electrically connected in series (situation from Figure 10a); (b) Voltage ( $U$ )-current ( $I$ ) and power ( $P$ )-current ( $I$ ) curves recorded for power source 2-kW PEMFC stack consisting of two fuel cell modules (1) and (2) which are electrically connected in series (situation from Figure 10a).

Figure 12a,b presents the electrical performance and temperature distribution  $T_1$  and  $T_2$  recorded under an applied electrical load of  $I = 48$  A for PEMFC stack modules (1) and (2) connected in parallel, where the cooling air flows through modules (1) and (2) arranged in series (situation from Figure 10a).

Figure 12a shows the current waveforms recorded for PEMFC modules (1) and (2), electrically connected in parallel, operating under an electric load of  $I = 48$  A. Based on Figure 12a, waveforms of different currents can be observed in modules (1) and (2), resulting from their different operating conditions. As shown by results from previous analyses of cooling conditions (Figure 10a), a lower operating temperature was recorded for module (1)— $T_1$  than for module (2)— $T_2$ . After switching on SCU<sub>1</sub> for module (1) and SCU<sub>2</sub> for module (2), momentary interferences can be observed during the measurement of current  $I$  and temperature  $t$ -values during self-moistening of the membranes in modules 1 and 2. This phenomenon is caused by changes in internal resistance. After a few seconds, both modules returned to the set operating conditions.



**Figure 12.** Cont.



**Figure 12.** (a) Waveforms of current originating from  $I_{m1}$ —module (1),  $I_{m2}$ —module (2) and temperature  $T$  during performance of the PEMFC stack with cooling air flow through modules (1) and (2) arranged in series (situation from Figure 10a). The electrical load applied was  $I = 48$  A. (b) Waveforms of power originating from  $P_{m1}$ —module (1),  $P_{m2}$ —module (2) and total power  $P = P_{m1} + P_{m2}$  from the PEMFC stack vs. time with cooling air flow through modules (1) and (2) arranged in parallel (situation from Figure 10b). The electrical load applied was  $I = 48$  A.

Figure 12b presents an increase in voltage  $U$  from 31 to 35 V for modules (1) and (2) connected electrically in parallel, caused by switching on  $SCU_1$  and  $SCU_2$ , which is the result of improved self-moistening of the electrolyte. The increase in voltage at a constant load of  $I = 48$  A also resulted in a corresponding increase in total output  $P$  from 1480 to 1670 W.

### 3.1.1. Comparison of Electrical Performance of the Designed Two-Module PEMFC Fuel Cell Stack with Other Commercial PEMFC Fuel Cell Stacks

To evaluate the performance of our designed fuel cell stack, we compared our results with those from other PEMFC fuel cell stacks with the same electrical power.

Figure 13 presents the  $U$ - $I$  and  $P$ - $I$  curves recorded for two different 2-kW PEMFC stacks, one constructed from two modules, (1) and (2),  $2 \times 1$  kW 2M (green points) connected in parallel; other commercial fuel cell stacks, HG (blue points) and BCH (red lines), characterized by power of 2 kW in one module, have been added for reference.

Based on an analysis of Figure 13, it can be concluded that the expected increase in current due to parallel electrical connections was observed in a comparison of current for single modules (1) and (2). According to Figure 13, nominal power output  $P_{nom}$  was obtained for a current-voltage pair close to  $I = \sim 75$  A and  $U = \sim 28$  V for power source (I), a 2-kW PEMFC stack consisting of two fuel cell modules (1) and (2) electrically connected in parallel. These data agree closely with the voltage values within the range 26–38 V assumed to be required for operation in a drone. Direct comparison of the performance of our two-module 2-kW PEMFC stack with that of commercial 2-kW PEMFC stacks enables us to state that higher values of current ( $I$ ) were obtained in the case of two-module electrical parallel connections of this kind. Moreover, as a result of direct comparison of the voltage ( $U$ )-current ( $I$ ) curve, a lesser decrease in voltage ( $U$ ) with increasing current ( $I$ ) was observed. These lesser decreases may be advantageous in the case of the integration of a PEMFC fuel cell stack with the  $U$ - $I$  characteristics of a Li-Po battery. These factors are important for the development of an energy management system in terms of increasing

battery life (through preventing rapid discharge) and increasing flight distance due to the potential for recharging the battery in flight.

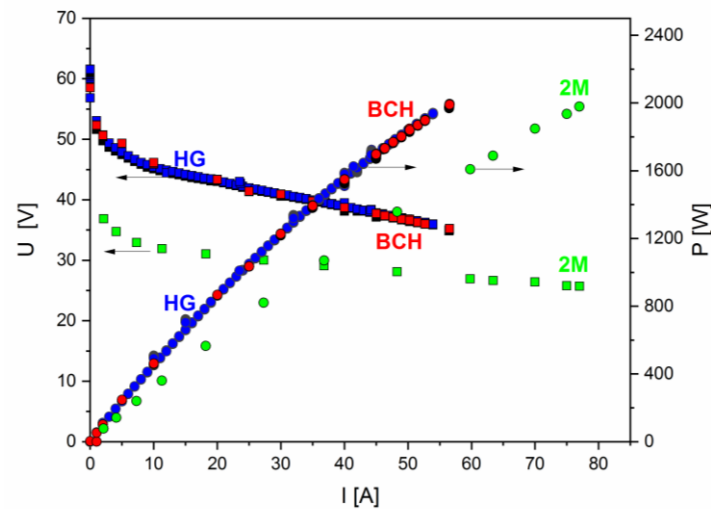


**Figure 13.** U-I and P-I curves recorded for three different 2-kW PEMFC stacks, one constructed from modules (1) and (2)— $2 \times 1$  kW—2M (green points) connected in parallel, and selected commercial fuel cell stacks, HG (blue points) BCH (red points) with power of 2 kW in a single module.

An additional advantage of this kind of two-module construction for a 2-kW PEMFC stack is that the modules are easier to position side by side such that the outlet of the cooling air being drawn between the two modules of the stack is directed evenly between the two sides. In the case of one module, the flow of the cooling air stream moves from one side to the other, which, for an airframe in which the stack of fuel cells is placed along the fuselage, would result in the formation of an additional unfavourable twisting moment that would hinder the drone from flying straight ahead.

Direction of the cooling air outlet from two stacks from the fuselage evenly to both sides results in reciprocal cancellation of the torsional moment and, as a result, no forces hinder straight flight. Chen et al. [45] analyzed the strategies of development of cooling technologies for a LT-PEMFC stack with electrical power ranging from 2 to 5 kW. According to these authors, air-cooled proton exchange membrane fuel cells are usually preferable below 1 kW, due to potentially limited development capacity. The main advantage of the application of an air-cooling system is its simpler construction and a lower consumption of power by the accessory system compared to a liquid cooling system. The main drawback of air-cooling systems in PEMFC fuel cells is that the maximum temperature difference throughout the stack can reach 9–14 °C. Nonuniform temperature distributions result in nonuniform performance distribution due to the ohmic and charge transfer resistance of individual MEA cells in the PEMFC stack along with temperature.

The variation of temperature ( $T_1$ ) and ( $T_2$ ) in both modules (1) and (2) vs. power is presented in Figure 14.

The maximum temperatures ( $T_{m1}$ ) and ( $T_{m2}$ ) in both modules were measured in the centre of the PEMFC stack. An increase in temperature  $T_{m1}$  or  $T_{m2}$  vs. electrical power was observed. The difference  $\Delta T$  measured in both PEMFC modules was no higher than 1–2 °C. These data also indicated that, due to limited dimensions and space, applications in drone construction may also constitute a prospective solution for installation of a cooling system.

The rational utilisation of hydrogen is also important for the application of PEMFC stacks in a hybrid propulsion unit. Firstly, the predicted duration of operation of a PEMFC stack during the flight of a drone depends on the amount of hydrogen stored in a composite bottle. The consumption of hydrogen vs. time varies with the electrical power and dynamic performance of the fuel cells.

Figure 15a presents the dependence of total hydrogen consumption when electrical power was produced by the two-module PEMFC stack.

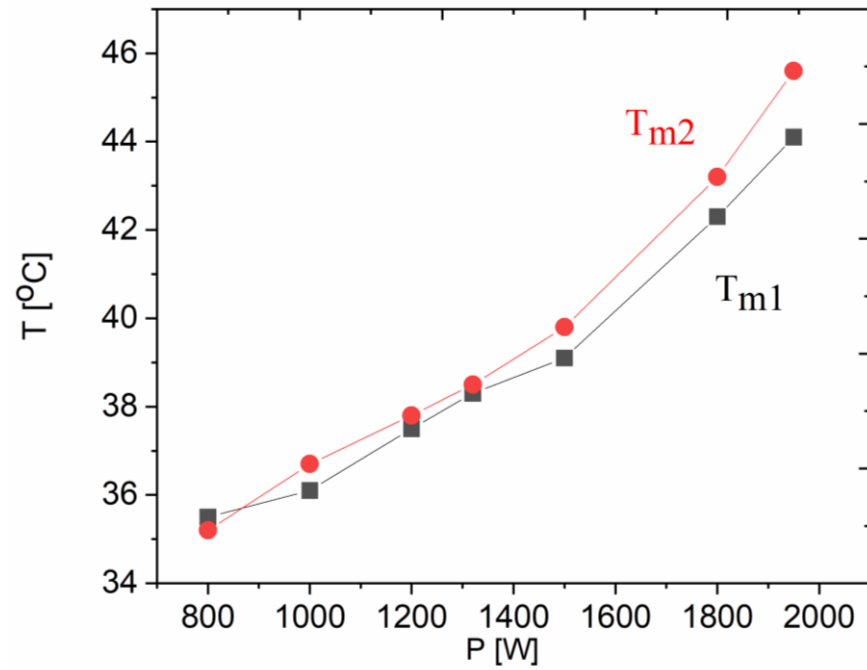


Figure 14. Variation in temperature T<sub>m1</sub> and T<sub>m2</sub> vs. electrical power (P) recorded for a 2-kW modular PEMFC stack.

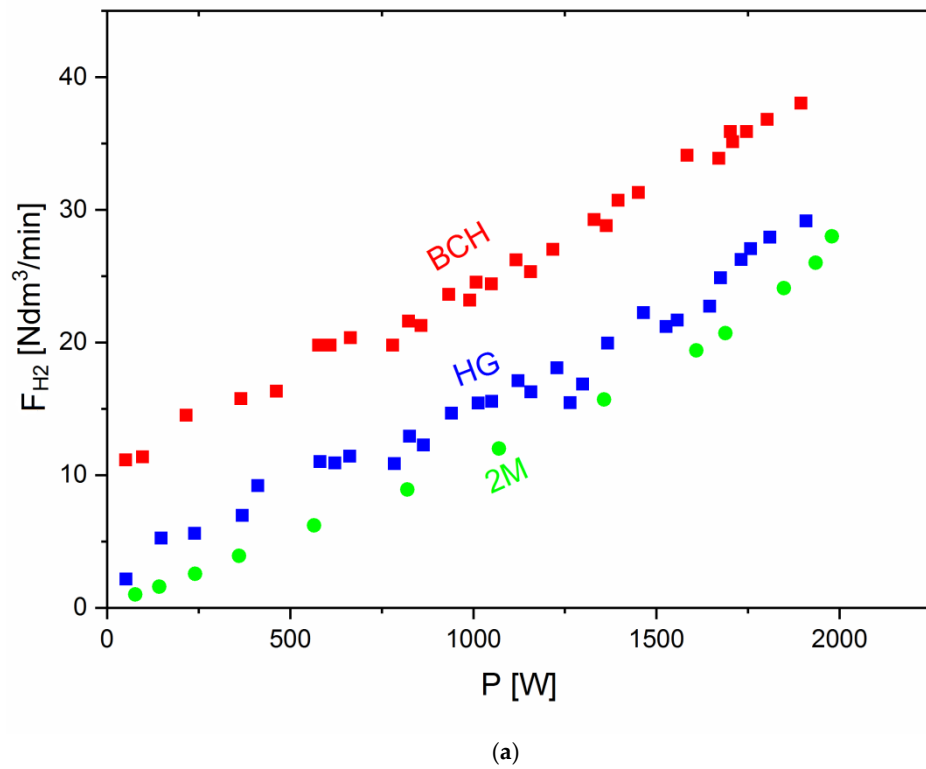
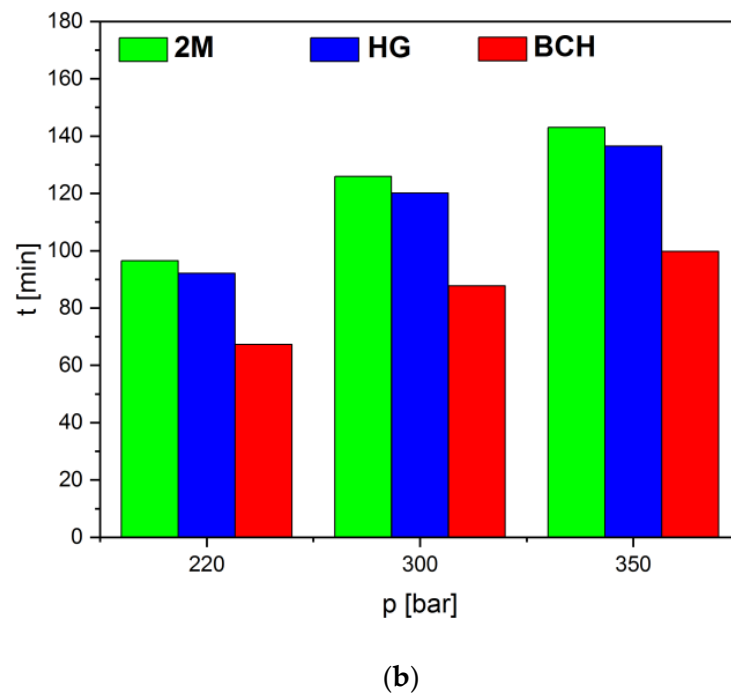


Figure 15. Cont.



**Figure 15.** (a) Comparison of hydrogen consumption  $F_{H_2}$  vs. power performance  $P$  of our designed 2-module fuel cell stack (2M) with other PEMFC fuel cell stacks, BCH and HG, with the same power of 2 kW. (b) Duration of 2-kW PEMFC stack operation for the same hydrogen storage. The hydrogen is compressed under 220, 300, and 350 bar of pressure in composite bottles ( $V = 13.6 \text{ dm}^3$ ).

The data recorded for the reference commercial PEMFC stacks with the same electrical power output of 2 kW is also presented. As can be seen, total hydrogen consumption increases with an increase in electrical power within the range 0–2000 W. A lower value of total hydrogen utilisation vs. electrical power was recorded for the PEMFC stack constructed from two 1-kW PEMFC modules (2M) compared to the PEMFC stack (BCH). In the case of comparison to the HG PEMFC stack, slightly lower consumption was also recorded.

As can be seen from Figure 15b, the longest duration of PEMFC fuel cell operation with nominal power of 2 kW is expected for the two-module PEMFC stack (2M). This duration is slightly greater than that recorded for the two analyzed reference 2-kW PEMFC stacks (HG, BCH) assembled as a single module. The main reason for the observed difference may be connected with the process of hydrogen purge operation according to the algorithm applied in PEMFC construction.

Figure 16 presents the electrical power required to supply the BOP devices (mainly cooling fans) vs. power produced by the PEMFC stack.

In further development research, a new geometry of metallic bipolar plates for a 2-module PEMFC stack may lead to a significant reduction in the overall mass of the PEMFC stack. It is expected that by replacing the graphite bipolar plates with metallic plates, the total mass can be reduced by about 50%; an increase in specific power density in the range of 500–550 W can be achieved, which is representative of a lightweight PEMFC stack with metallic bipolar plates.

On the other hand, the achieved power density W/kg for a 2-kW PEMFC stack is  $\sim 270 \text{ W/kg}$ , and the specific power density of whole hydrogen system (calculated as the sum of the mass of a complete 2-module PEMFC stack and the lightweight composite cylinders with the entire hydrogen gas infrastructure) is  $\sim 133 \text{ W/kg}$ . This value fits well within the range of a commercial PEMFC stack with graphite bipolar plates [19,46].

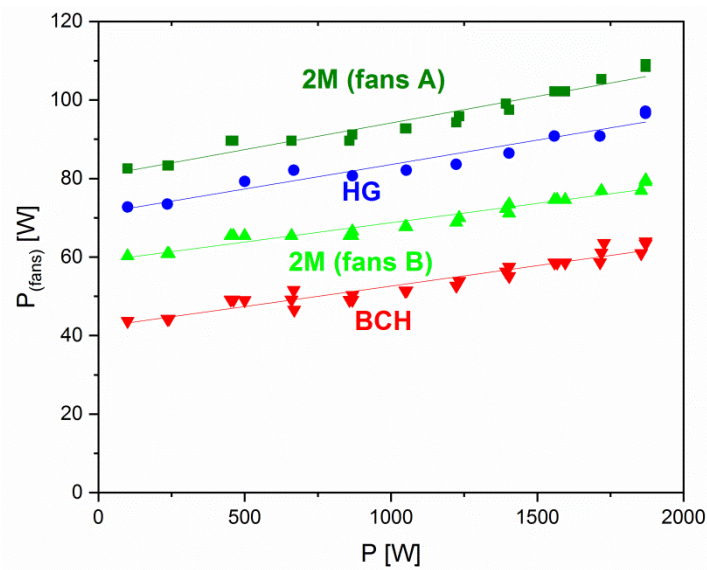


**Figure 16.** Measured electrical power  $P_{fan}$  needed to supply the cooling system vs. electrical power produced by the 2-kW PEMFC stack, where 2M represents the two-module fuel cell stack and HG represents the H 2000 PEMFC fuel cell stack (Horizon, Singapore), and BCH Energy 2000 W.

### 3.1.2. Test of the Electrical Performance of the Designed Two-Module PEMFC Fuel Cell Stack with a Propeller Connected to a BLDC Motor

The PEMFC stack was integrated into a propulsion system involving a BLDC motor with a  $30 \times 12$  propeller, as depicted in Figure 4.

Figure 17a,b present the U-I, P-I, curves recorded for the investigated propulsion unit (a) and dependence of the rotational speed of a  $30 \times 12$  propeller connected to a BLDC motor vs. power (b) respectively. In Figure 17a the dependence of total hydrogen consumption  $F_H$  (Ndm<sup>3</sup>/min) vs. current (I) was also added.

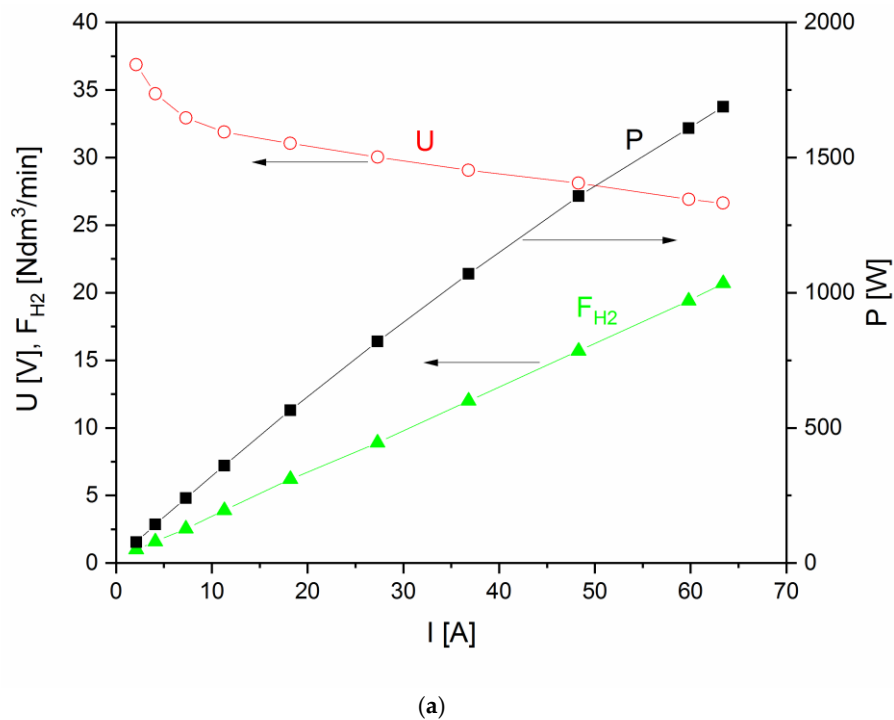
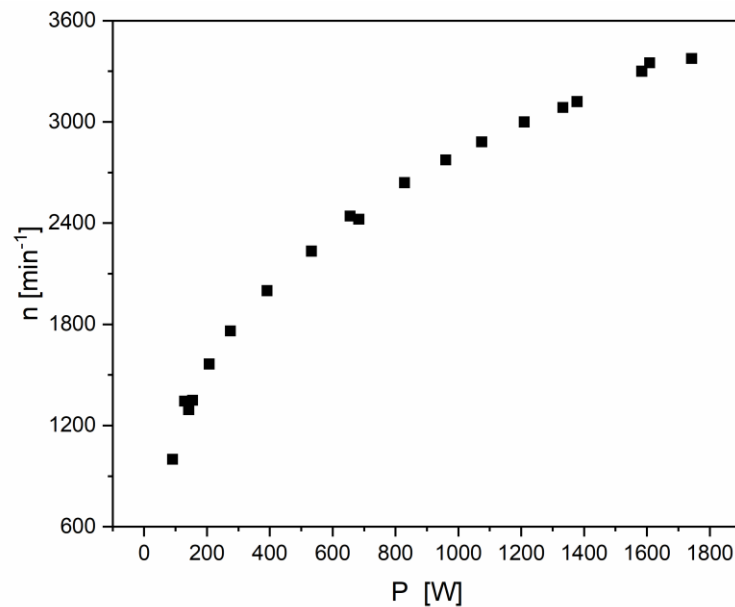


**Figure 17.** Cont.



(b)

**Figure 17.** (a) The U-I; P-I and  $F_H$ -I curves recorded for the investigated 2-kW PEMFC stack integrated in propulsion unit (according to a scheme from Figure 4). (b) Dependence of the rotational speed of a  $30 \times 12$  propeller connected to a BLDC motor vs. power.

Depending on the setting of the motor control signal, the rotations varied within a range of approximately 800–3400 revolutions/min with an increase in the electric power drawn by the engine within the range of approximately 100–1750 W. These results showed that the designed and constructed 2-kW PEMFC stack appears to be of value for additional investigation into the propulsion unit.

### 3.2. Electrical Tests of the 500-W PEMFC Stack

The second type of PEMFC stack mentioned was a three-module 500-W power source designed as a power supply for on-board electronic and executive devices (servomechanisms, motors, electromagnets). These devices, which also require an uninterrupted supply of electricity during their operation, are characterized by a variable profile of power demand throughout operation.

Figure 18 presents the U-I and P-I curves recorded for the three-module 500-W PEMFC stack. As can be seen, the designed PEMFC operated within an approximate variable voltage range of 21–33 V, and within a current range of 0–25 A.

The nominal power output  $P_{\max}$  of the PEMFC stack was recorded for a U-I pair ( $\sim 21$  V;  $\sim 25$  A), and corresponded to maximum power P of  $\sim 515$  W. No characteristic maximum point of power was observed in the P-I curve. The assembled PEMFC stack was also capable of supplying excess power for a short time. These results confirmed that the 500-W modular PEMFC stack could be tested in an electrical connection with a hybrid electrochemical power source (a 500-W three-module PEMFC stack with a parallel connection to a 2250-mAh 5 s lithium-polymer battery).

The electrical behavior of the hybrid power source 5 s lithium polymer battery plus 500 W PEMFC stack was also studied. The combined effect of supporting the hydrogen-oxygen fuel cells from 5 s lithium-polymer battery during higher power demand is shown in Figure 19.

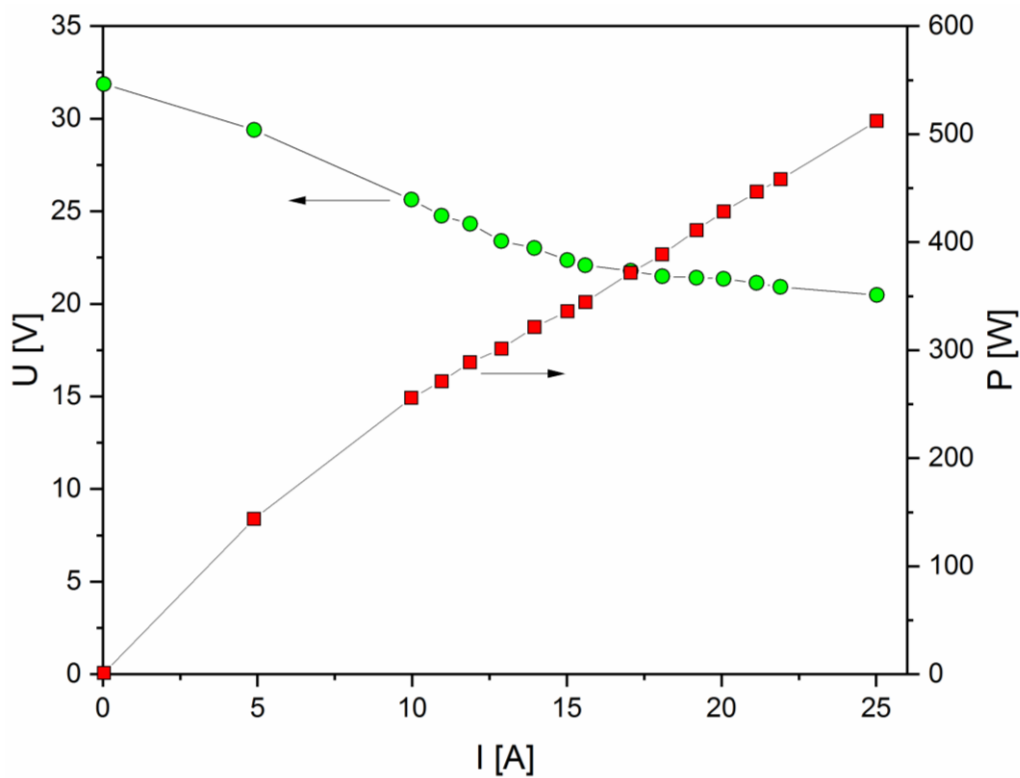


Figure 18. Voltage (U)-current (I) curve, or power P vs. current I recorded for the three-module PEMFC stack.

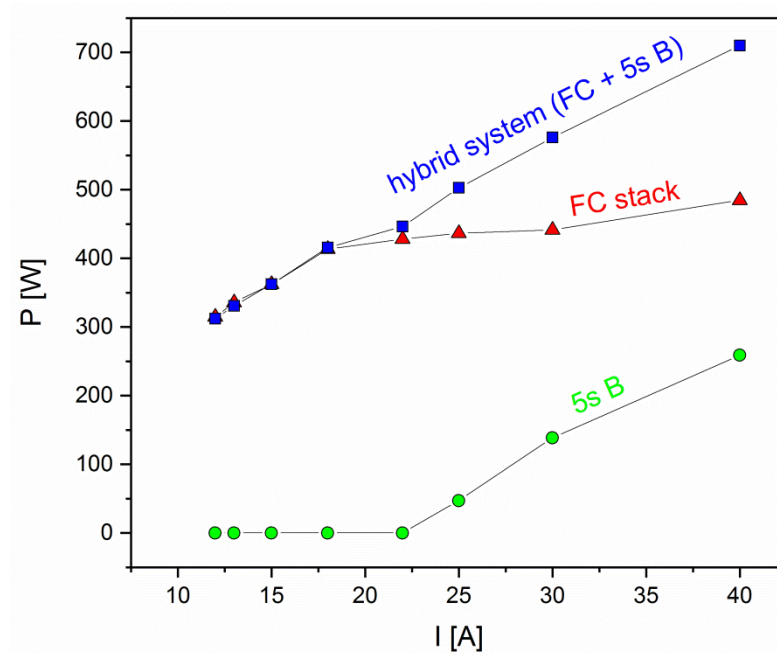
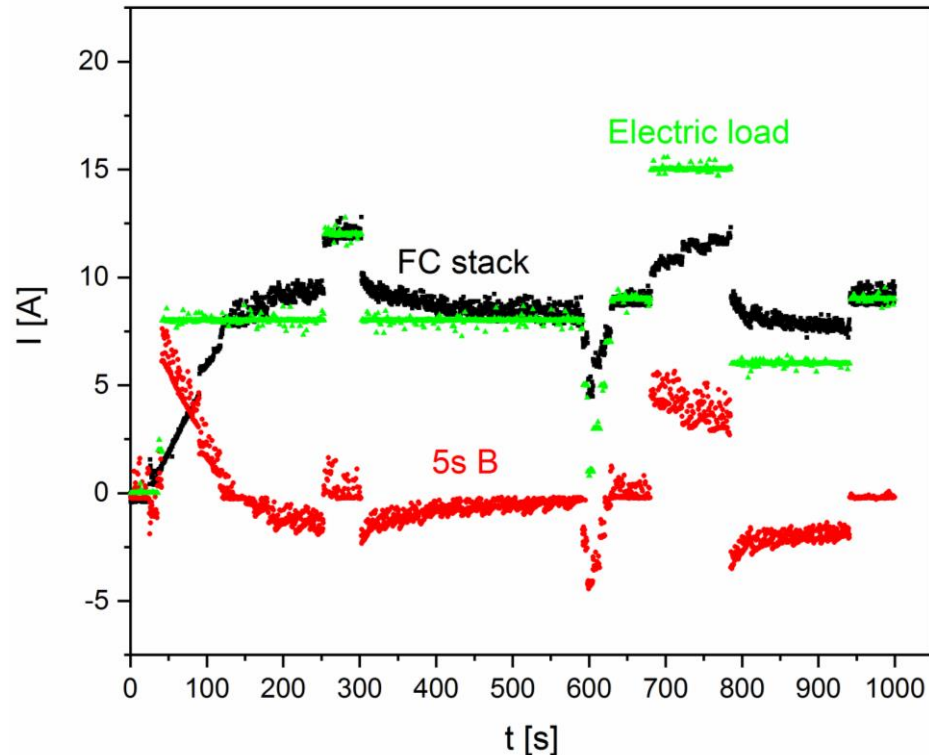


Figure 19. Power (P)-current (I) distribution recorded for a hybrid power source consisting of a three-module PEMFC stack (FC) and 5s lithium-polymer battery (5s B).

In the case of a slow increase in electrical load within the current range  $I = 0\text{--}22\text{ A}$ , the power was mainly supplied from the modular PEMFC stack. When the current (I) was increased above 22 A, power was also supplied from the electrochemical battery power source. The total power of the hybrid power sources recorded in these conditions was 710 W; in the case of the PEMFC stack alone, 490 W. The increase in the power of the hybrid power source was confirmed by this study.

In Figure 20 the current vs. time waveforms recorded during constant current mode operation of a three-module 500-W stack of fuel cells integrated with a lithium-polymer battery (5s B) is presented.



**Figure 20.** Current vs. time waveforms recorded during the operation of a three-module 500-W stack of fuel cells integrated with an electrochemical battery (5s B) under current load within the range 0–15 A, where: green line—load—current taken from hybrid system (500-W fuel cell stack + LiPo 5s battery pack) by electronic load; red line—battery—current taken from LiPo 5s battery pack; black line—current taken from 500-W fuel cell stack (FC stack).

The system was loaded in the constant current mode within a range of 0–15 A. Approximately 50 s after starting the PEMFC stack, the power source was loaded with a constant current of 8 A. At that time, a gradual increase in the current drawn from the 500-W PEMFC stack and a simultaneous decrease in the current drawn from the electrochemical battery was observed. In the case of the battery, the current stabilized below 0 A (−2 A), signifying recharging of the battery. The slow increase in the current produced from the PEMFC stack resulted from the need to warm the stack up to the set operating temperature and from the gradual increase in electrolyte hydration. The stepwise increase in the current electronic load to 12 (time from 250 to 300 s) or 15 A (time from 700 to 800 s) resulted in a similar response on the part of the cell's current; however, in these cases, the current flowing from the battery stabilized above 0 A and the current taken from the battery reached ~2 A (time from 250 to 300 s) and ~4 A (time from 700 to 800 s), which was associated with gradual discharge of the battery.

Hybrid power sources consisting of simultaneous (parallel) mutually independent PEMFC stacks and electrochemical batteries provide so-called double power, which ensures the redundancy of the power sources such that in the event of the failure of one, the other can still supply power to a limited extent, i.e., the second functional module can still operate and deliver the power at its disposal. Operation of this kind is of particular importance in aviation applications for such critical systems as avionics and the control and powering of servo systems governing control functions (the airframe remains under control and can be steered, which will enable it, for example, to make an emergency landing in glider mode

after losing its propeller function). Low-temperature PEMFC stacks consist of many cells connected in series. The operation of a power source containing a PEMFC stack requires the simultaneous correct operation of all components in the stack. In extreme cases, damage to even a single cell in the PEMFC stack may lead to its complete shutdown. The reliability of such a power source can be enhanced by using independently operating smaller stacks (modules) of fuel cells.

Figure 21 presents the variation in distribution of current flowing from individual modules connected in parallel under various electrical loads. This may occur in cases where some MEA cells in PEMFC modules are characterized, for various reasons, by lower values of electrical properties. In cases of nonuniform temperature distributions, MEA cells with modules with hot-spot operations are expected to exhibit poorer performance due to the potential presence of some pinholes which may occur under operation in such conditions. These defects may reduce the voltage of membranes, which may also lead to changes in the directions of polarization, or to electrical short circuits in the PEMFC stack.

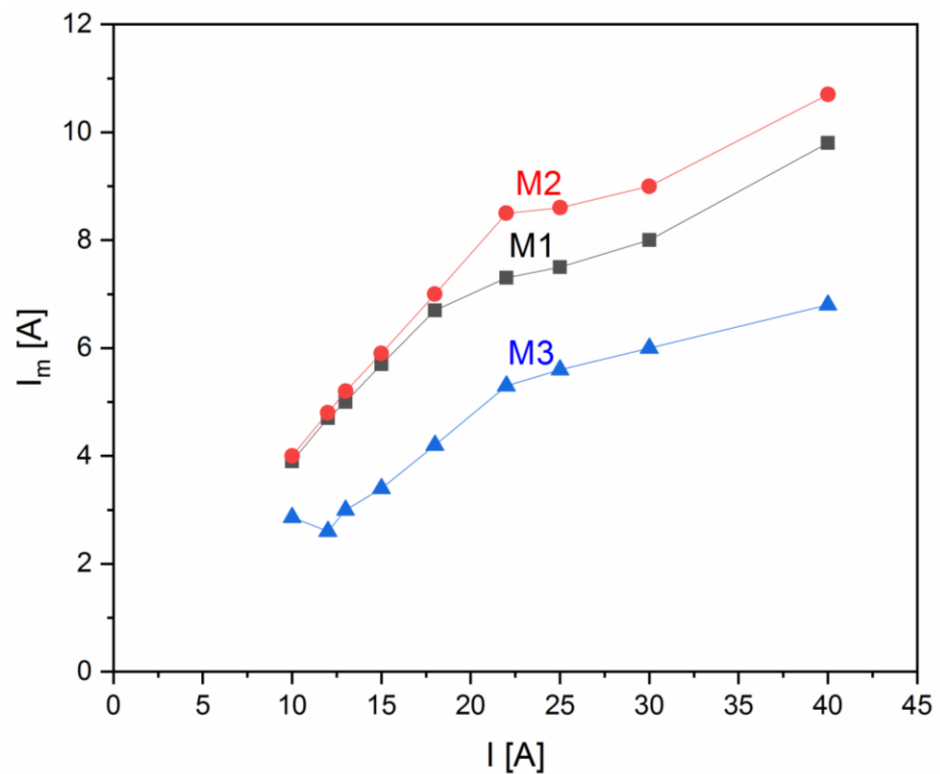


**Figure 21.** Variation in the distribution of current flowing from individual modules (M1; M2; M3) connected in parallel in 500 W PEMFC stack under various electrical loads.

These unfavorable phenomena may, in a single-module PEMFC stack, lead to devices integrated within the energy systems (e.g., DC/DC converters) being turned off. Nonuniform temperature distributions also lead to the presence of various stresses. Under nonuniform stress the risk of cracks and pinholes in fuel cell components becomes relatively high. The flooding phenomenon may also result in unstable PEMFC stack performance. One possible reason for this was a suboptimal humidification process, in which more water was produced than expected. In such situations, poor performance can be observed, especially during an increase in current density [47]. In the case of PEMFC stack application, the reliability and monitoring of these parameters are very important for propulsion structures as well as for as the power source supplying BOP in the drones.

From the analysis of the data presented in Figure 21, it can be seen that the intensity of the current drawn from the two modules (1, 2) is comparable and, at the same time, greater than the intensity of the current drawn from module (3). This variation in behavior

is probably connected with the lower values of some MEA cells and differences in their humidity. In order to circumvent these problems, in the segmented power source, the electrical power generated by different sections in the modular fuel cell stack can be independently controlled in hybrid power sources. During electrical loads, given certain faults in the module, the energy management system is capable of reducing power; alternatively, the faulty stack section can be shut down. Assumptions have been developed for technical supervision procedures and the flight safety of hydrogen-powered drones. Redundant fuel cell power sources were tested in order to supply electrical devices.

Simultaneous parallel operation of the fuel cell modules and the electrochemical battery connected passively (by means of blocking diodes) increases the operational reliability of electrochemical power sources [33,48]. In a passive parallel connection, electricity is initially drawn from a higher voltage source. The increase in load, and thus the voltage drop, equalizes the voltages of the connected sources and starts their simultaneous operation. The load distribution between individual sources working in parallel is automatic and does not require an additional control and control system or additional DC/DC converters, which would increase losses, demand for auxiliary power and increase the weight of the energy source.

The waveform of electrical power ( $P$ ) vs. time recorded during the operation of single servomechanism powered directly from the electric power source involving a 500-W modular PEMFC fuel cell stack is presented in Figure 22.

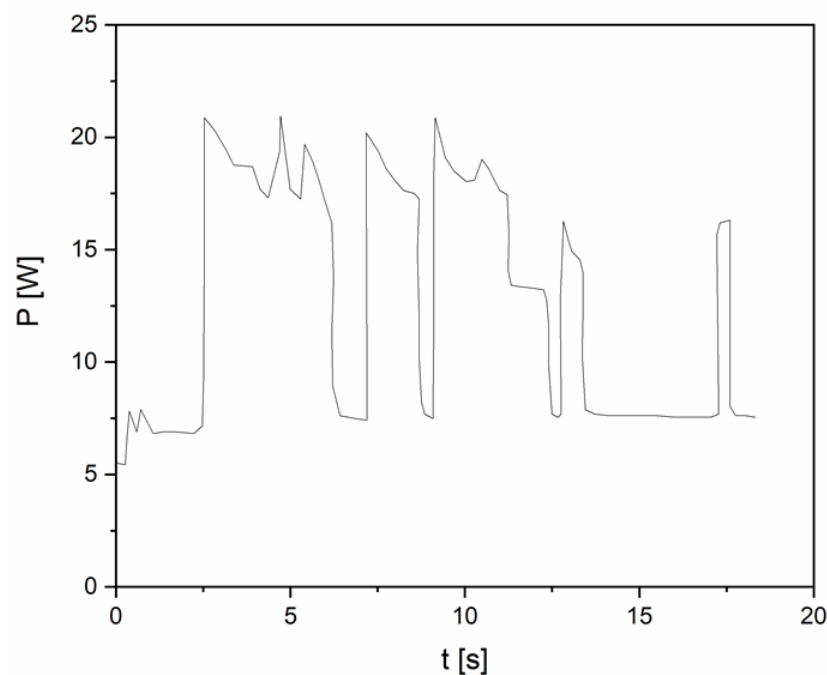


**Figure 22.** The waveform of electrical power ( $P$ ) vs. time recorded during the operation of servomechanisms powered directly from the electric power source involving a 500-W modular PEMFC fuel cell stack.

These data were recorded during the variation of the steering angle, at which time the set servomechanism position was maintained. The servomechanisms, unlike the propulsion engine, were characterized by lower, albeit dynamic, variations in electric load. This resulted from the need to change the position as quickly as possible and to maintain the new set position. These tests confirmed the required dynamic PEMFC performance. On the other hand, in Figure 22 the waveform of electrical power ( $P$ ) vs. time recorded during the operation of servomechanisms powered directly from the electric power source involving a 500-W modular PEMFC fuel cell stack. The investigation of the electrical output of 500 W PEMFC stack during step changes was also performed.

In Figure 23 the waveform power  $P$  vs. time during the variable loads were also recorded under dynamic variable electrical load. In this investigation the electrical output of 500 W PEMFC stack during step changes was investigated.

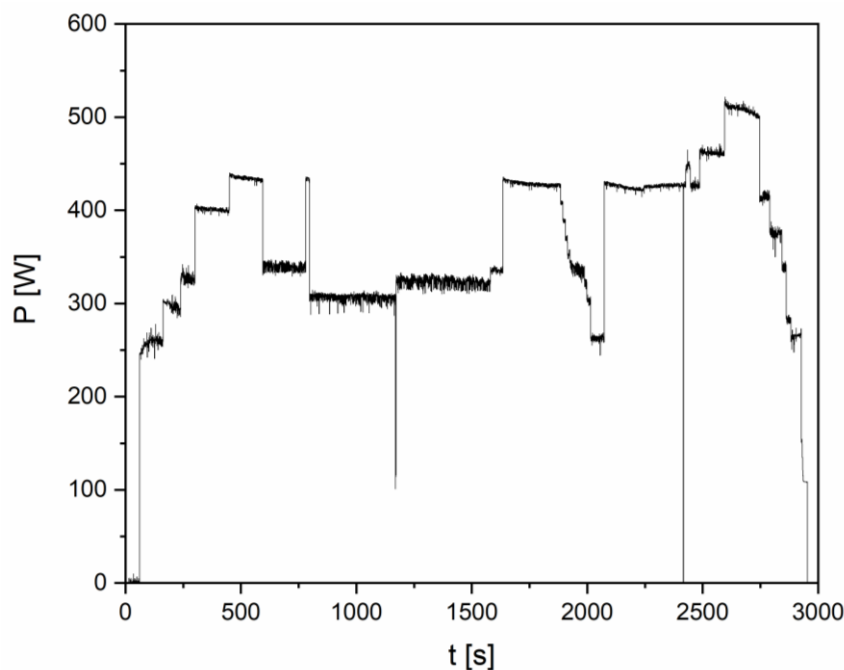


**Figure 23.** The waveform of electrical power ( $P$ ) vs. time recorded during the operation of servomechanisms powered directly from the electric power source involving a 500-W modular PEMFC fuel cell stack.

In the first part of the experiment, a rapid increase of electrical power from 0 to 250 W, followed by an increase of power up to 450 W, was observed from 20 to 600 s. In the last stage of the test, electrical power varied within the range 250–500 W for 2000 s. It was found that the constructed PEMFC stack was capable of supplying the required power ranging from 0–500 W in a timely fashion in accordance with the variation of dynamic loads during the performance of servomechanisms.

#### 4. Conclusions

The study provides an analysis of the feasibility of constructing multimodule power sources containing fuel cell stacks for supplying power to the electric motor and on-board equipment of an unmanned aerial vehicle. The 2-kW PEMFC stack consisted of two 1-kW PEMFC modules electrically connected in parallel. It was found that, according to the assumed electrical operation parameters in the propulsion unit, the nominal power output  $P_{nom}$  corresponded to the following pair of electrical parameters:  $I = \sim 75$  A,  $U = \sim 28$  V. Direct comparison of the electrical parameters of the 2-kW two-module PEMFC stack compared to those of the 2-kW single-module PEMFC stack indicated that construction of these power sources in modular forms enabled the acquisition of greater current density as well as a reduced need for power to supply fans and reduced hydrogen consumption. The feasibility of integrating the two-module PEMFC stack into a propulsion unit involving a BLDC electrical engine connected with a propeller was demonstrated. All of these features are important for applications and can serve as alternative solutions. A 500-W three-module PEMFC stack was designed, constructed, and tested. This stack was also characterized by electrical power output suited to the required electrical system of the BOP. Investigations of the performance of the designed hybrid power source, i.e., the 500-W PEMFC stack with an electrical battery, were also performed. The durability of the 500-W PEMFC stack was also discussed and demonstrated. Special attention was devoted to the safe operation of

power sources involving hydrogen, based on redundancy, control monitoring parameters, and easier operation despite the existence of some defaults. It was concluded that the use of modular fuel cell stacks makes it possible to construct power sources adjusted to the electrical loads required for energy systems used aboard unmanned aerial vehicles.

**Author Contributions:** M.D.: conception of the paper, writing, original draft preparation, supervision and interpretation of experimental parts, contributions to all experimental parts, resources, data curation; B.L.: design and construction of modular PEMFC stacks, electrical measurements of the power sources described in the paper, graphs; A.R.: contributions to electrical measurements, analysis of cooling system, data curation; M.K. (Michał Kawalec): construction of PEMFCs, electrical measurements, data curation, preparation of graphs; M.K. (Mariusz Krauz): project leader, supervision, contributions to all experimental parts. All authors have read and agreed to the published version of the manuscript.

**Funding:** The National Centre for Research and Development, Warsaw, Poland, No. INNOLOT/I/3/NCBR/2013 HYBRIDRIVE—“Technology of hybrid power package for powering light or unmanned aerial vehicles”.

**Institutional Review Board Statement:** Not applicable.

**Informed Consent Statement:** Not applicable.

**Data Availability Statement:** It does not apply to this work.

**Acknowledgments:** The study received support as part of the sector project INNOLOT HYBRIDRIVE—“Technology of hybrid power package for powering light or unmanned aerial vehicles”. Part of the research was conducted using the research infrastructure of the Centre of Energy of the AGH University of Science and Technology.

**Conflicts of Interest:** The authors declare no conflict of interest.

## Abbreviations

FC	fuel cells
M <sub>i</sub>	PEMFC module; i = 1; 2; 3
PEMFC	polymer membrane fuel cells
5s Li-Pol	lithium polymer battery contained 5 cells connected in series
UAVs	unmanned aerial vehicles
MEA	membrane electrode assembly
GDL	gas diffusion layers
SOC	state of charge
MCFC	multistack fuel cell
DC	direct constant current
EIS	electrochemical impedance spectroscopy
EEC	equivalent electrical circuit
CPE	constant phase element
BOP	balance of fuel cell power plant
F <sub>H2</sub>	hydrogen intensity flow (Ndm <sup>3</sup> /min)
R <sub>Ω</sub>	ohmic resistance spectroscopy
R <sub>ct</sub>	charge transfer resistance
R <sub>m</sub>	mass transport resistance
R <sub>t</sub>	total electrical resistance
HG	2-kW PEMFC stack with graphite bipolar plate (product H series, Horizon Fuel Cell Technologies Pte Ltd; Singapore)
BCH	2 kW BCH Energy (Jiangsu Ice-City Hydrogen Energy Technology Co., Ltd., Danyang, China)
2M	2-kW PEMFC stack consisting of two fuel cell modules,
BLDC	brushless direct-current motor
MCU	microcontroller system units
T <sub>m1</sub>	temperature; PEMFC module 1
T <sub>m2</sub>	temperature; PEMFC module 2

$P_{fan}$	electrical power needed to supply the cooling system
$U$	voltage
$I$	current
$I_m$	current of PEMFC module fuel cell stack
$U_{m1}$	voltage, PEMFC module 1
$U_{m2}$	voltage, PEMFC module 2
$P_{m1}$	power, PEMFC module 1
$P_{m2}$	power, PEMFC module 2
$Q$	heat
$V$	stream of air
$\rho$	the air density
$C_{pp}$	the specific heat of the air
SCU	short-circuit units
PC	personal computer
$Z'$	real part of impedance plot
$Z''$	imaginary part of impedance plot

## References

- Hassanalain, M.; Abdelkefi, A. Classifications, applications, and design challenges of drones: A review. *Prog. Aerosp. Sci.* **2017**, *91*, 99–131. [CrossRef]
- Outay, F.; Mengash, H.A.; Adnan, M. Applications of unmanned aerial vehicle (UAV) in road safety, traffic and highway infrastructure management: Recent advances and challenges. *Transp. Res. Part A Policy Pract.* **2020**, *141*, 116–129. [CrossRef] [PubMed]
- Mishra, B.; Garg, D.; Narang, P.; Mishra, V. Drone-surveillance for search and rescue in natural disaster. *Comput. Commun.* **2020**, *156*, 1–10. [CrossRef]
- Alzahrani, B.; Oubbati, O.S.; Barnawi, A.; Atiquzzaman, M.; Alghazzawi, D. UAV assistance paradigm: State-of-the-art in applications and challenges. *J. Netw. Comput. Appl.* **2020**, *166*, 10270. [CrossRef]
- Aydin, B. Public acceptance of drones: Knowledge, attitudes, and practice. *Technol. Soc.* **2019**, *59*, 101180. [CrossRef]
- Nouacer, R.; Hussein, M.; Espinoza, H.; Ouhammou, Y.; Ladeira, M.; Castiñeira, R. Towards a framework of key technologies for drones. *MiCrap. Microsyst.* **2020**, *77*, 103142. [CrossRef]
- Vilbig, J.M.; Sagan, V.; Bodine, C. Archaeological surveying with airborne LiDAR and UAV photogrammetry: A comparative analysis at Cahokia Mounds. *J. Archaeol. Sci. Rep.* **2020**, *33*, 102509.
- Zhang, M.; Li, S.; Yu, F.; Tian, X. Image fusion employing adaptive spectral-spatial gradient sparse regularization in UAV remote sensing. *Signal Process.* **2020**, *170*, 107434. [CrossRef]
- Kim, S.J.; Lim, G.J.; Cho, J. Drone flight scheduling under uncertainty on battery duration and air temperature. *Comput. Ind. Eng.* **2018**, *117*, 291–302. [CrossRef]
- Sato, M.; Nirei, M.; Yamanaka, Y.; Suzuki, T.; Bu, Y.; Mizuno, T. Increasing the efficiency of a drone motor by arranging magnetic sheets to winding. *Energy Rep.* **2020**, *6*, 439–446. [CrossRef]
- UAV—Fuel Cell Solutions Ballard Power. Available online: <https://www.ballard.com/markets/uav> (accessed on 20 November 2020).
- Osenar, P.; Sisco, J.; Reid, C. *Advanced Propulsion for Small Unmanned Aerial Vehicles—The Role of Fuel Cell-Based Energy Systems for Commercial UAVs*; Protonex Technology Corporation: Southborough, MA, USA, 2017.
- Depcik, C.; Cassidy, T.; Collicott, B.; Burugupally, S.P.; Li, X.; Alam, S.S.; Arandia, J.R.; Hobeck, J. Comparison of lithium ion Batteries, hydrogen fueled combustion Engines, and a hydrogen fuel cell in powering a small Unmanned Aerial Vehicle. *Energy Convers. Manag.* **2020**, *207*, 112514. [CrossRef]
- Bayrak, Z.U.; Kaya, U.; Oksuztepe, E. Investigation of PEMFC performance for cruising hybrid powered fixed-wing electric UAV in different temperatures. *Int. J. Hydrog. Energy* **2020**, *45*, 7036–7045. [CrossRef]
- Giacoppo, G.; Barbera, O.; Briguglio, N.; Cipiti, F.; Ferraro, M.; Brunaccini, G.; Erdle, E.; Antonucci, V. Thermal study of a SOFC system integration in a fuselage of a hybrid electric mini UAV. *Int. J. Hydrog. Energy* **2017**, *42*, 28022–28033. [CrossRef]
- Dudek, M.; Raźniak, A.; Lis, B.; Siwek, T.; Adamczyk, B.; Uhl, D.; Kalawa, W.; Uhl, T. Monitoring of the operating parameters a low-temperature fuel-cell stack for applications in unmanned aerial vehicles: Part I. *E3S Web Conf.* **2019**, *108*, 01029. [CrossRef]
- Dudek, M.; Raźniak, A.; Lis, B.; Siwek, T.; Adamczyk, B.; Uhl, D.; Kalawa, W.; Uhl, T. Monitoring of the operating parameters a low-temperature fuel-cell stack for applications in unmanned aerial vehicles: Part II. *E3S Web Conf.* **2019**, *108*, 01030. [CrossRef]
- Kwon, S.; Kang, S.; Kim, T. Development of NaBH<sub>4</sub>-Based Hydrogen Generator for Fuel Cell Unmanned Aerial Vehicles with Movable Fuel Cartridge. *Energy Procedia* **2019**, *158*, 1930–1935. [CrossRef]
- Gong, A.; Verstraete, D. Fuel cell propulsion in small fixed-wing unmanned aerial vehicles: Current status and research needs. *Int. J. Hydrog. Energy* **2017**, *42*, 21311–22133. [CrossRef]

20. Wang, B.; Zhao, D.; Li, W.; Wang, Z.; Huang, Y.; You, Y.; Becker, S. Current technologies and challenges of applying fuel cell hybrid propulsion systems in unmanned aerial vehicles. *Prog. Aerosp. Sci.* **2020**, *116*, 100620. [CrossRef]
21. Boukoberine, M.N.; Zhou, Z.; Benbouzid, M. A critical review on unmanned aerial vehicles power supply and energy management: Solutions, strategies, and prospects. *Appl. Energy* **2019**, *255*, 113823. [CrossRef]
22. Verstraete, D.; Lehmkuehler, K.; Gong, A.; Harvey, J.R.; Brian, G. Characterisation of a hybrid, fuel-cell-based propulsion system for small unmanned aircraft. *J. Power Sources* **2014**, *250*, 204–211. [CrossRef]
23. Dudek, M.; Tomczyk, P.; Wygonik, P.; Korkosz, M.; Bogusz, P.; Lis, B. Hybrid Fuel Cell—Battery System as a Main Power Unit for Small Unmanned Aerial Vehicles (UAV). *Int. J. Electrochem. Sci.* **2013**, *8*, 8442–8463.
24. Lei, T.; Yan, Z.; Lin, Z.; Zhang, X. State of art on energy management strategy for hybrid-powered unmanned aerial vehicle. *Chin. J. Aeronaut.* **2019**, *32*, 1488–1533. [CrossRef]
25. Zhang, X.; Liu, L.; Dai, Y.; Lu, T. Experimental investigation on the on line fuzzy energy management of hybrid fuel cell/battery power system for UAVs. *Int. J. Hydrog. Energy* **2018**, *43*, 10094–10103. [CrossRef]
26. Ballard turnkey fuel cell solutions to power commercial UAVs. *Fuel Cells Bull.* **2019**, *5*, 6. Available online: <https://www.ballard.com/about-ballard/newsroom/news-releases/2019/04/29/ballard-launches-turnkey-fuel-cell-solutions-to-power-commercial-unmanned-aerial-vehicles> (accessed on 11 January 2021).
27. Horizon-Raptor UAS tie-up aims for 300 km fuel cell UAV flight. *Fuel Cells Bull.* **2015**, *9*, 3.
28. Intelligent Energy launches 2.4 kW fuel cell module for UAVs. *Fuel Cells Bull.* **2019**, *5*, 6.
29. Energy or fuel cell multicopter drone in 2 h flight with camera. *Fuel Cells Bull.* **2016**, *2*, 3–4. Available online: <https://www.sciencedirect.com/science/article/abs/pii/S146428591670006X> (accessed on 11 January 2021).
30. Chinese UAV maker MMC flies hydrogen fuel cell drone for 4 h. *Fuel Cells Bull.* **2016**, *6*, 4–5.
31. Li, M.; Bai, Y.; Zhang, C.; Song, Y.; Jiang, S.; Grouset, D.; Zhang, M. Review on the research of hydrogen storage system fast refueling in fuel cell vehicle. *Int. J. Hydrog. Energy* **2019**, *44*, 10677–10693. [CrossRef]
32. Oh, T.K. Conceptual design of small unmanned aerial vehicle with proton exchange membrane fuel cell system for long endurance mission. *Energy Convers. Manag.* **2018**, *17*, 6349–6356.
33. Renau, J.; Schanzes, S.; Lozano, A.; Barroso, J.; Barreras, F. Analysis of the performance of a passive hybrid power plant to power a lightweight unmanned aerial vehicle for a high altitude mission. *J. Power Sources* **2017**, *356*, 124–132. [CrossRef]
34. Kang, H.; Kim, S.Y. Thermal design analysis of a 1 L cryogenic liquid hydrogen tank for an unmanned aerial vehicle. *Int. J. Hydrog. Energy* **2014**, *39*, 20009–20016. [CrossRef]
35. Palma, L.; Enjeti, P.N. A modular fuel cell, modular DC–DC converter concept for high performance and enhanced reliability. *IEEE Trans. Power Electron.* **2009**, *24*, 1437–1443. [CrossRef]
36. Marx, N.; Boulon, L.; Gustin, F.; Hissel, D.; Agbossu, K. A review of multi stack and modular fuel cell systems: Interest, application area and on-going research activities. *Int. J. Hydrog. Energy* **2014**, *39*, 12101–12111. [CrossRef]
37. Giaccoppo, G.; Hovland, S.; Barbera, O. 2 kW Modular PEM fuel cell stack for space applications: Development and test for operation under relevant conditions. *Appl. Energy* **2019**, *242*, 1683–1696. [CrossRef]
38. Segura, F.; Andújar, J.M. Modular PEM Fuel Cell SCADA & Simulator System. *Resources* **2015**, *4*, 692–712.
39. Dudek, M.; Raźniak, A.; Rosół, M.; Siwek, T.; Dudek, P. Design, development, and performance of a 10 kW polymer exchange membrane fuel cell stack as part of a hybrid power source designed to supply a motor glider. *Energies* **2020**, *13*, 4393. [CrossRef]
40. Rathke, P.; Thalau, O.; Kallo, J.; Schirmer, J.; Stephan, T. Long distance flight testing with the fuel cell powered aircraft Antares DLR-H2. In Proceedings of the Deutscher Luft und Raumfahrtkongress 2013, Stuttgart, Germany, 10–12 September 2013. Available online: <https://www.dglr.de/publikationen/2014/301219.pdf> (accessed on 18 December 2020).
41. Jiangsu Ice-City Hydrogen Energy Technology Co., Ltd. Available online: <http://www.hydrogenpowered-fuelcells.com/aboutus.html> (accessed on 18 December 2018).
42. Air Cooled Stacks Horizon Fuel Cell Technologies. Available online: <http://www.horizonfuelcell.com/hseries> (accessed on 25 December 2020).
43. Yan, X.; Hou, M.; Sun, L.; Liang, D.; Shen, Q.; Xu, H.; Ming, P.; Yi, B. AC impedance characterisation of a 2 kW PEM fuel cell stack under different operation conditions and load changes. *Int. J. Hydrog. Energy* **2007**, *32*, 4358–4364. [CrossRef]
44. Seed, A.; Mokmeli, A.; Samavati, M. Study of PEM fuel cell performance by electrochemical impedance spectroscopy. *Int. J. Hydrog. Energy* **2010**, *35*, 9283–9290.
45. Chen, C.Y.; Huang, K.P.; Yan, W.M.; Lai, M.P.; Yang, C.C. Development and performance diagnosis of a high power air-cooled PEMFC stack. *Int. J. Hydrog. Energy* **2016**, *41*, 11784–11793. [CrossRef]
46. Bradley, T.; Moffitt, B.; Parekh, D.; Mavris, D. Flight test results for a fuel cell unmanned aerial vehicle. In Proceedings of the 45th AIAA Aerospace Sciences Meeting, Reno, NV, USA, 8–11 January 2007; pp. 254–261.
47. Shen, J.; Xu, L.; Chan, H.; Tu, Z.; Chan, S.H. Partial flooding and its effect on the performance of a proton exchange membrane fuel cell. *Energy Convers. Manag.* **2020**, *207*, 112537. [CrossRef]
48. Nishizawa, A.; Kallo, J.; Garrot, O.; Weiss-Ungethüm, J. Fuel cell and Li-ion battery direct hybridization system for aircraft applications. *J. Power Sources* **2013**, *222*, 294–300. [CrossRef]